CHAPTER 4

RESULTS AND DISCUSSION

4.1 Characterisation of kaolin before and after modification

4.1.1 X-ray diffraction (XRD)

1. Composition of the Natural Ranong kaolin

The mineralogy of the Natural Ranong kaolin (NK) was investigated by powder X-ray diffraction using Ni-filtered CuK_α radiation (λ= 1.54 nm). Diffraction patterns were collected in the range of $2\theta = 5^\circ$ to 60° at a scanning speed 1° per 2θ/min, and working at 40 kV/40 mA. Mineral components in the X-ray diffractogram were identified by comparison with standards in the JCPDS Powder Diffraction File. The XRD pattern of Natural Ranong kaolin is illustrated in Figure 4.1.

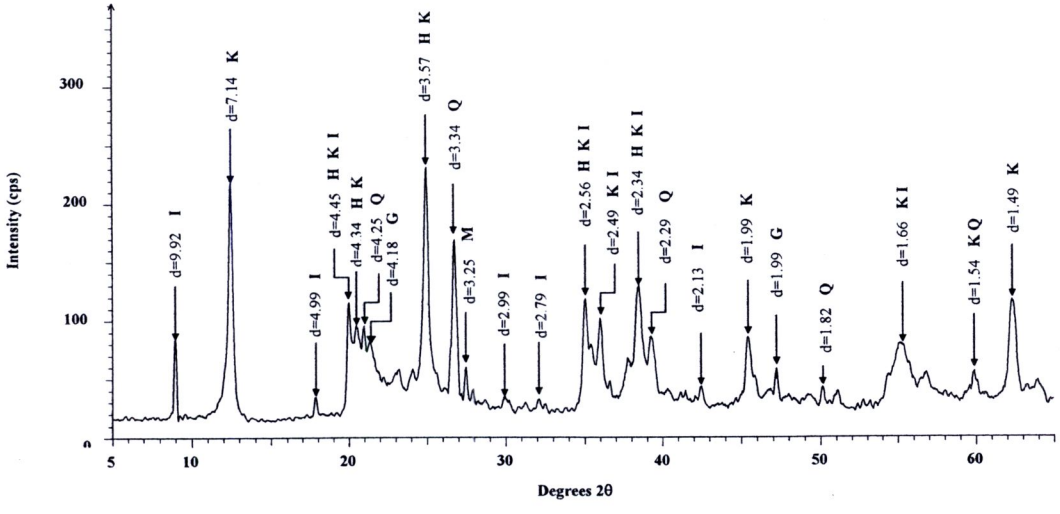

Figure 4.1 Powder X-ray diffraction patterns of Natural Ranong kaolin (NK), and the assignment to its component minerals. K = kaolinite, H = halloysite, Q = quartz, I = illite, G = goethite and M = microcline

The majority of the peaks can be accounted for by the kaolin minerals; the strong peaks at 7.14, 3.57 and 1.49Å correspond to the kaolinite *d*(001), *d*(002) and *d*(060) reflections and the peaks at 4.45, 2.56, 2.49, 2.34, 1.99, 1.66, and 1.49 are all consistent with kaolinite. Positive identification of halloysite from these data is difficult, because the main peaks from halloysite-10 Å at 10Å and halloysite-7 Å at 4.42 Å both overlap

with peaks from illite, and the peak at 4.34 Å can correspond to either halloysite or kaolinite (Brindley & Brown 1980). Illite, which is a common impurity in kaolin-minerals, is present in appreciable quantities in the Ranong kaolin, as seen by the presence of major peaks at 9.92 and 2.56 Å in addition to those mentioned above. Other peaks consistent with illite are observed at 4.99 and 2.99 Å. The presence of quartz is seen by its principal reflection at 3.34 Å, and associated minor peaks at 4.25, 2.29, 1.82, and 1.54 Å. In addition, weak peaks at 4.18 and 3.25 Å could correspond to the main reflections from goethite and microcline, respectively, so these minerals may be present as minor impurities, but the absence of other diffraction peaks prevents a positive identification.

The clay mineral groups are distinguished by the behaviour of their characteristic basal reflections in response to various chemical and heat treatments (Figure 4.2). The insensitivity of the peaks at ~10.0 Å to ethylene glycol, and heating to 550 °C means that they correspond at least mainly to the *d*(001) reflections from illite, and that halloysite-10 Å makes only a minor contribution (if any) to their intensity. Both halloysite-7 Å and kaolinite are unaffected by glycolation, but become amorphous to X-rays after heating to 550 °C, and Figure 4.2 shows the conversion of peaks at *d*~ 7 Å and ~3.5 Å to an amorphous phase at ~12.38°2θ at this temperature. Finally, since intercalation with formamide results in an increase in the *d*(001) reflection of halloysite-7 Å to ~ 10.0 Å, the peak at 7.17 Å in the original kaolin corresponds primarily to halloysite. These results are thus qualitatively similar to those reported by Nuntiya and Prasanphan (2006) for their kaolin sample from Ranong, but the sample in the present work contained smaller amounts of impurity phases. The Hinkley index (HI) (Hinckley, 1963) of about 0.32 suggests that the kaolinite is of only moderate crystallinity, whereas both the FTIR and EPR results (**Sections 4.1.3 and 4.1.4**) indicate that the mineral is well-ordered. However, Brindley et al., (1986) report that the HI is directly correlated with kaolinite-Fe content, so its relationship to crystallinity may be complicated by isomorphous substitutions. Furthermore, the presence of overlapping peaks from illite and quartz with those of kaolinite used for measuring the HI complicates its accuracy for kaolinite crystallinity determination in the present sample.

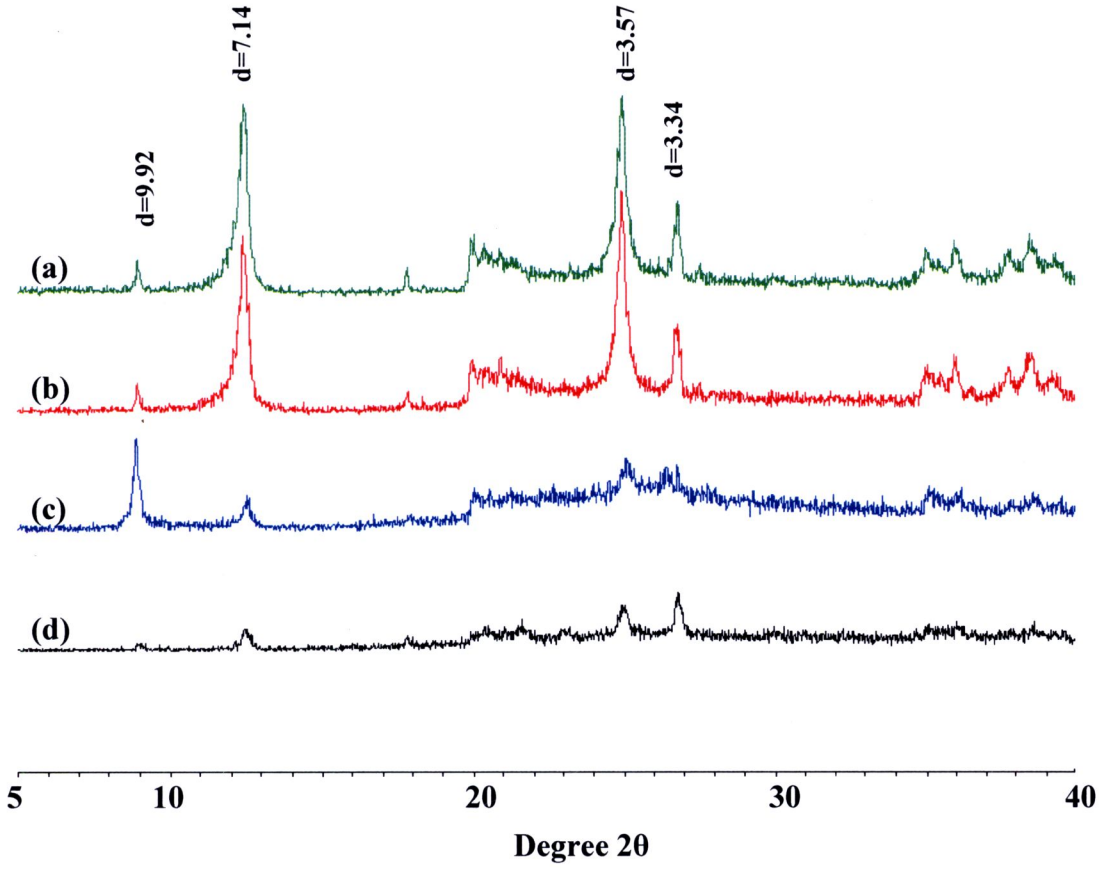

Figure 4.2 Powder X-ray diffraction patterns of oriented kaolin (a) as a result of air drying (b) glycolation (c) intercalation with formamide, and (d) heating to 550 °C.

2. Influence of individual chemical and physical treatments on the kaolin crystallinity

XRD patterns for Ranong kaolin before and after grinding or sulfuric acid treatment are shown in Figure 4.3. They show that the kaolin minerals are resistant to the acid treatment, (UGKS 2 and UGKS 3.7 Figures 4.3(b and c)), since the *d*(001) reflection at 7.14 Å, the *d*(002) reflection at 3.57 Å, and the *d*(060) reflection at 1.48 Å remained intense and sharp, even under strongly acidic conditions (FWHM data in Table 1). However, grinding the clay resulted in a major decrease in the relative intensities of the kaolin mineral and illite phases (sample GK, Figure 4.3(d)), consistent with appreciable structural damage to these minerals. Furthermore, there was also an increase in the background in the 20-30°2θ range that is typical of the presence of amorphous phases.

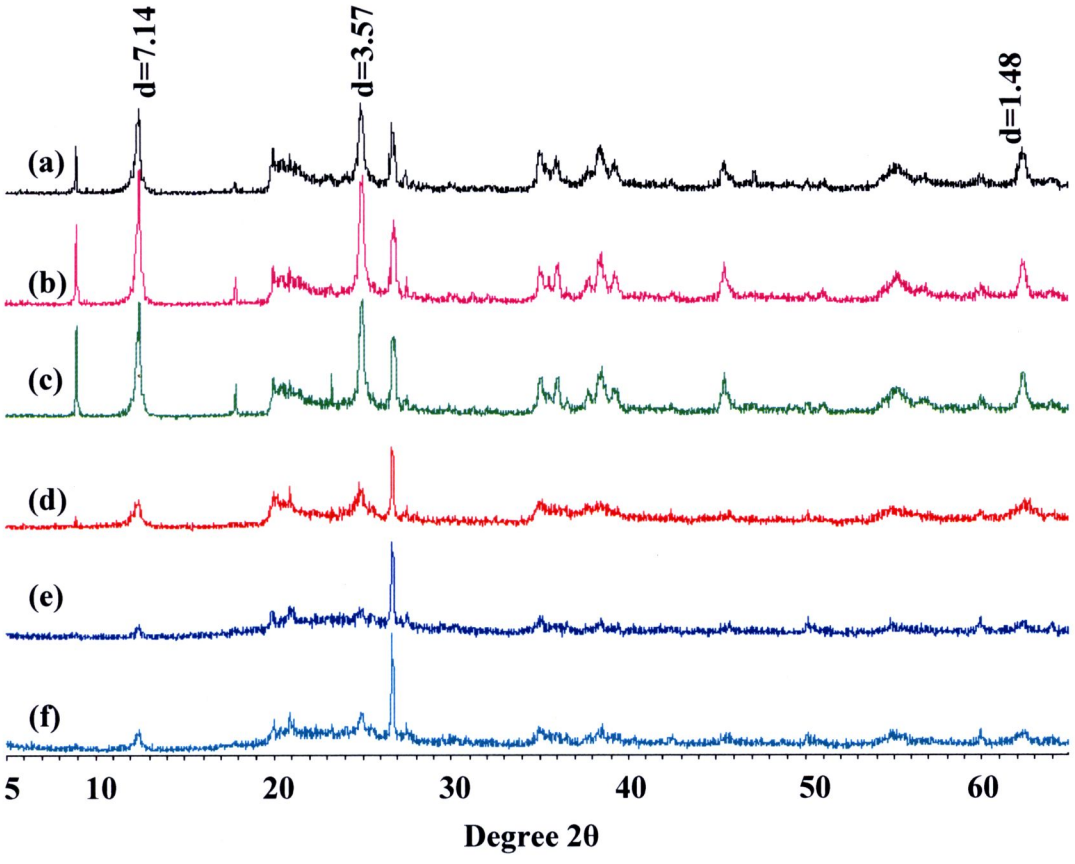

Figure 4.3 Powder X-ray diffraction patterns for (a) Natural Ranong kaolin (NK) and modified samples UGKS 2 (b) UGKS 3.7 (c) GK (d) GKS 2 (e), and (f) GKO 0.7. Peaks corresponding to the identified mineral phases are shown on the diffractogram of the untreated sample.

Using the Scherrer formula (Langford and Wilson, 1978), the FWHM data for *d*(001) indicates that the mean number of layers in a kaolinite stack is ~90 for samples NK, UGKS 2 and UGKS 3.7. This value decreases to ~70 (i.e. a reduction of ~25%) after grinding, but then increases again to ~ 90 for GKS18 and GKO6. Grinding had little effect on the *d*(060) peak, and samples NK and GK both have ~380 planes in a stack. However, it is of great importance after acid attack with the number of layers in the *b* dimension decreasing to ~280 for UGKS 2 and UGKS 3.7, and ~190 for GKS 2 and GKO 0.7.

3. Effects of combined physical and chemical treatments

Further changes in the XRD patterns were observed after treating the ground sample with either sulfuric or oxalic acids, GKS 2 and GKO 0.7 (Figures 4.3(e) and (f)); apart from the peak at ~26.74° 2θ, which probably corresponds to quartz, there is an appreciable reduction in intensity in all regions. Aluminium compounds resulting from grinding-induced kaolin breakdown were removed by the acid treatments as indicated by the XRF results (see **Section 4.1.2**), presumably as a result of the formation of soluble Al salts. Although the peaks corresponding to the kaolinite/halloysite minerals were very weak in these XRD spectra, they were still quite sharp (Table 4.1), suggesting that the residual fraction of these minerals is relatively unaltered.

Table 4.1 Variation of positions and linewidths of the main kaolinite XRD peaks in the various Ranong kaolin samples

Sample	*d*(001)	FWHM	*d*(002)	FWHM	*d*(060)	FWHM
NK	7.09	0.27	3.56	0.29	1.49	0.32
UGKS 2	7.11	0.29	3.56	0.32	1.49	0.44
UGKS 3.7	7.12	0.27	3.57	0.28	1.49	0.42
GK	7.15	0.37	3.57	0.41	1.49	0.31
GKS 2	7.15	0.27	3.57	0.40	1.49	0.60
GKO 0.7	7.14	0.28	3.57	0.31	1.49	0.69

4.1.2 X-ray fluorescence (XRF) analyses

Table 2 shows the major elements determined by XRF analyses of the original kaolin, the original and ground kaolins treated with 2 M sulfuric acid and the ground kaolin treated with 0.7 M oxalic acid. Si and Al are the dominant elements in the original kaolin, along with minor amounts of K and Fe; the concentrations of Mn, Ti, Mg and Ca are all quite small. Decreases in the Al:Si and Fe:Si ratios were observed as a result of acid treatment of the unground clay, but much larger decreases were observed after acid leaching the ground kaolin. Since the main minerals in the sample are halloysite, kaolinite, illite and quartz, along with minor amounts of mica and orthoclase and iron oxides, it is possible to use the data in Table 2 to get a rough idea of the composition of the samples. By using the theoretical chemical compositions for these phases, and attributing all of the Al to kaolinite/halloysite, we find that this component accounts for ~85% of the original kaolin sample, and this decreases to ~40% in GKS. In ground and

acid-treated products, the main phase is probably amorphous silica (≤50%) which is consistent with the strong development of Si-O bands in the FTIR spectra (see **Section 4.1.3**). Thus these results suggest that there was selective removal by acid of some phases generated as a result of structural breakdown induced by prolonged grinding. Therefore, the physical treatment followed by chemical treatment may be a promising process for kaolin modification.

Table 4.2 Chemical composition of Ranong kaolin samples determined by X-ray fluorescence

Oxide (% mass)	Sample			
	NK	UGKS 2	GKS 2	GKO 0.7
SiO_2	46.70	51.40	72.77	67.84
Al_2O_3	37.90	33.63	13.50	16.13
K_2O	1.23	1.46	1.48	1.51
Fe_2O_3	0.54	0.41	0.29	0.27
MnO	0.04	0.03	0.03	0.03
TiO_2	0.03	0.02	0.03	0.03
CaO	0.01	0.01	ND	ND
MgO	0.03	0.03	0.03	0.02
Na_2O	0.03	0.03	0.04	0.04
LOI	13.49	12.90	11.76	14.09
Al:Si[a]	0.95	0.77	0.22	0.28
Fe:Si[a]	0.85%	0.60%	0.27%	0.30%

[a] atomic ratios
ND = not detected
NK = Natural kaolinite
UGKS = Unground kaolinite followed by sulfuric acid treatment
GKS 2 = ground kaolinite followed by 2 M sulfuric acid treatment
GKO 0.7 = ground kaolinite followed by 0.7 M sulfuric acid treatment

4.1.3 Fourier Transform Infrared Spectroscopy (FTIR) studies

The full range FTIR spectra of the kaolin samples are shown in Fig. 4.4 to illustrate the relative intensities of the peaks in the different regions of the spectra.

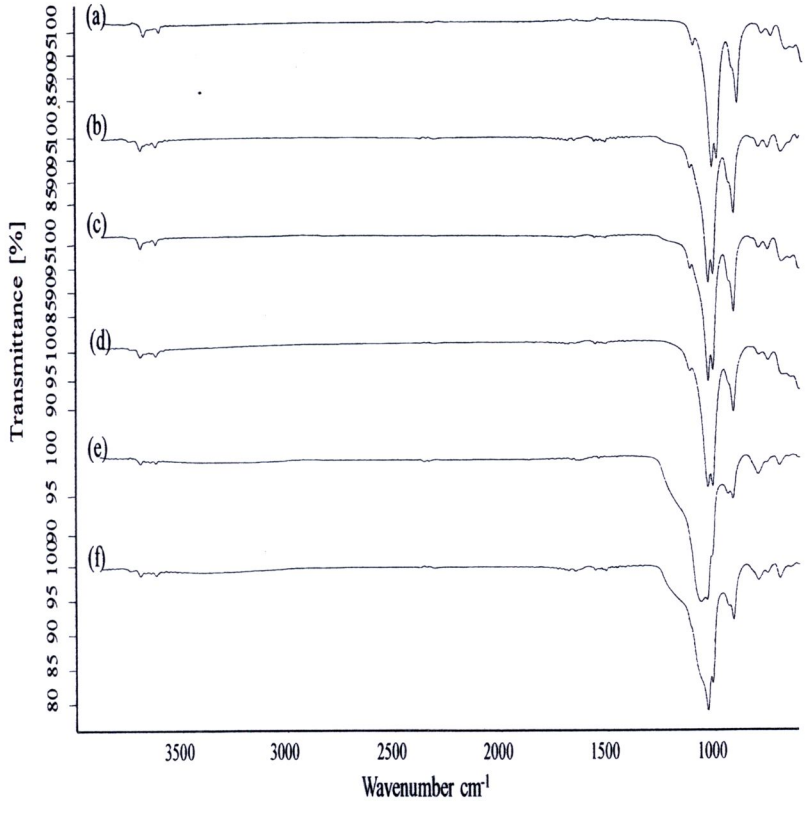

Figure 4.4 FTIR spectra of Ranong kaolin samples (a) untreated kaolin (NK), and treated at 90 °C for 4 h with (b) 2 M or (c) 3.7 M H_2SO_4, (d) NK ground for 1 h, and then treated with (e) 2 M H_2SO_4, or (f) 0.7 $H_2C_2O_4$ at 90 °C for 4 h.

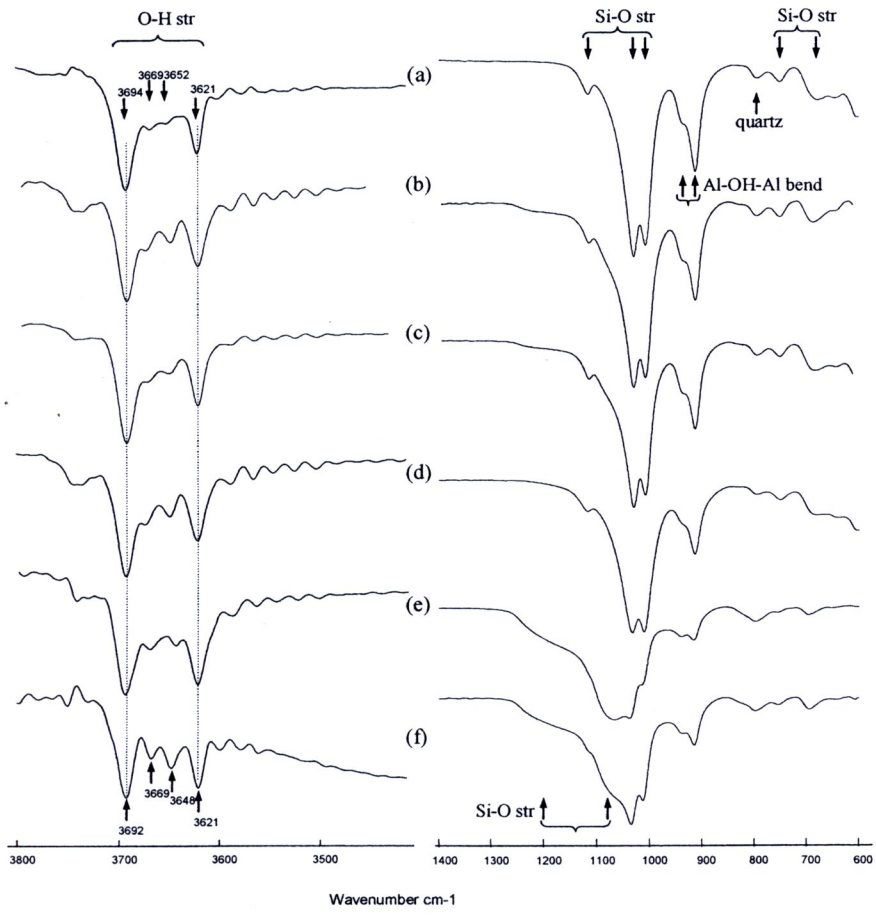

Figure 4.5 Expansion of the main absorption regions in the FTIR spectra of Ranong kaolin samples (a) untreated kaolin (NK), and treated at 90 °C for 4 h with (b) 2 M or (c) 3.7 M H_2SO_4, (d) NK ground for 1 h, and then treated with (e) 2 M H_2SO_4, or (f) 0.7 M $H_2C_2O_4$ at 90 °C for 4 h.

The main absorptions in the FTIR spectra of the kaolin samples are shown in Figure 4.5. In the original kaolin sample, NK, The O-H stretching vibrations consist of two well-defined peaks at 3694 and 3621 cm^{-1} flanking two weaker peaks at 3669 and 3652 cm^{-1}. This spectrum is typical of kaolinite, (*e.g.* van der Marel and Krohmer (1969) report bands at 3693, 3668, 3652 and 3620 cm^{-1}). In contrast to the HI from the XRD results, the good resolution of these peaks suggests that the mineral is quite well-ordered, and provides support for the analysis of the *d*(001) and *d*(060) peaks in the XRD results. As proposed by Farmer (1974, 1998), and subsequently confirmed by theoretical

calculations (Balan *et al.*, 2005), the band at the lowest wavenumber corresponds to vibrations of the inner OH group, that at the highest wavenumber to the in-phase motion of the three surface OH groups, and those at intermediate positions to out-of-phase motion of these groups.

The bands at ~935 and 913 cm^{-1} correspond to the inner surface and inner Al-OH-Al bending vibrations (Farmer and Russell, 1964) and those at 1116, 1030 and 1007 cm^{-1} to Si-O stretching vibrations in kaolinite/halloysite, but there was only a hint of a shoulder at ~1100 cm^{-1} where the Si-O (apical) band is expected (*e.g.* Frost *et al.*, 2002). The band at 1030 cm^{-1} could also contain a contribution from muscovite, which was detected by Nuntiya and Prasanphan (2006) as an impurity in their Ranong kaolin, but was not seen in the XRD patterns from our present sample. The peak at 793 cm^{-1} is probably associated with quartz, which was identified as an impurity in the XRD traces of both Nuntiya and Prasanphan (2006) and the present work. There was no evidence for discrete absorption at ~3425 cm^{-1}, the frequency at which the O-H stretching vibration occurs in smectites, other common impurities in kaolin minerals. The bands at 751 and 687 cm^{-1} correspond to those assigned to Si-O stretching vibrations (Ekosse, 2005).

Little change was observed in the spectra as a result of sulfuric acid treatment, (Figure 4.5(b and c)) indicating that the kaolin minerals are resistant to acid treatment, although weak new peaks were seen at ~1220 and 828 cm^{-1} and a shoulder at ~1075 cm^{-1}; since peaks were observed in these positions, but with higher intensity, in the ground samples after acid treatments, they indicate that the acid treatment did induce some modification of the unground kaolin. There was also some decrease in the relative intensities of the bands at ~935 and 913 cm^{-1} from Al-OH-Al bending vibrations. In contrast, grinding reduced the intensities of the kaolinite O-H stretching vibration bands by ~65% (Figure 4.5(a,d)), indicating that physical modification of the mineral was accompanied by extensive dehydroxylation as observed by Miller and Oulton (1970). However, the Al-OH-Al bending vibration bands were reduced by a smaller amount, and the O-H and Al-OH-Al peaks that remained after grinding were unshifted. Thus, they indicate that the kaolinite that remained was essentially unaltered from that in the original sample.

Frost *et al.* (2001a, b) have also reported IR results for a mechanochemically treated kaolinite, in which there were both similarities and differences from the measurements reported above. Both our measurements and those of Frost *et al.* showed decreases in the intensity of the OH stretching vibrations (3695 and 3619 cm^{-1}) and deformation modes (935 and 913 cm^{-1}), but Frost *et al.* also observed an increase in the bending mode at 1650 cm^{-1} from water bound to the surface of the modified kaolinite; this was extremely weak in the present measurements (probably because of the drying of the sample). Also, whereas we observed little change in the Si-O stretching vibrations, Frost *et al.* reported a significant reduction in intensity that was accompanied by an increase in a new band at 1113 cm^{-1}, which was assigned to the surface of the newly synthesized product. It should also be noted that the Si-O stretching vibrations reported by Frost *et al.* (2001b) were at 1034 and 1056 cm^{-1}, which are considerably higher than the values of 1011 and 1030 cm^{-1} that were observed in the present work.

Acid treatment of the ground sample did not produce any further changes in the OH stretching frequencies, and the differences in the relative intensities of the peaks are not considered significant because of the low overall intensity in this region of the spectra. There were, however, appreciable changes in other regions of the spectra. The intensities of the Al-OH-Al bending vibrations were reduced, and are roughly correlated with the reduction in the Al content (Table 4.2). There were also significant differences in the relative intensities of new bands in the sulfuric and oxalic acid treated samples, although their positions were similar (Table 4.3). Intense broad bands generated at ~1205 cm-1 and 1067 or 1077 cm^{-1} (depending on the acid used) probably correspond to Si-O stretching bands associated with newly synthesized material, since weak bands in similar positions were observed in the spectra of the unground clay after acid treatment. These are significantly different from the results reported by Frost *et al.* (2001), who described the formation of a new band at 1113 cm^{-1}; the narrow peak at 1117 cm^{-1} in the natural kaolin (and at 1121 cm^{-1} in the ground sample) in the present work, was lost completely on acid treatment in experiments of Frost *et al.* (2001a,b, 2002, 2003, 2004). However these authors found that the presence of quartz increased appreciably the rate of grinding induced breakdown of the kaolinite, and this may also be a factor in the determining the physical characteristics of the breakdown products.

There was a reduction in the relative intensities of the Si-O deformation bands, which occurred at 1007 and 1030 cm^{-1} in the original kaolin sample, and these were also shifted to slightly higher wavenumbers after grinding and acid treatment, but overall the changes in this region of the spectrum were relatively minor. Larger changes were observed with the Al-OH-Al bending vibrations at 935 and 913 cm^{-1}; although their intensities were reduced after grinding, much greater additional reductions were apparent after the acid treatment, consistent with dissolution of the octahedral sheet which contains most of the O-H groups.

Table 4.3 FTIR frequencies and assignments in Ranong kaolin samples

NK	UGKS 2	UGKS 3.7	GK	GKS 2	GKO 0.7	Assignment
3694	3692	3692	3695	3692	3692	O-H
3669	3674	3672	3670	3669	3669	
3652	3649	3650	3646	3648	3648	
3621	3621	3621	3623	3621	3621	
				3397 (v broad)	3346 (v broad)	O-H
~1650	1654	1650	1650	1646	1650	Surface water
~1560			1632	1633	1634	
	~1220	~1220		1205	1205	Si-O
1116	1116	1116	1116	1116	1116	Si-O
	~1075	~1075			1077	
1030	1030	1030	1033	1067	1035	
1007	1007	1007	1011	1036	1013	
				1011		
935	935	935	935	940	937	Al-OH-Al
913	913	913	913	916	914	
	828	828		828	828	
793	796	794	794	796	796	quartz
751	751	751	751	754	754	Si-O
687	687	687	687	696	696	
648	647	647	648	649	642	

4.1.4 Electron paramagnetic resonance (EPR) spectroscopy

The wide scan EPR spectra of the Ranong kaolin before and after grinding are shown in Figure 4.6. As is common for clay mineral samples with relatively low overall contents of paramagnetic ions, these spectra contain signals from four different sources; (i) a group of peaks in the field range 50-250 mT which originate from isolated Fe^{3+} ions, (ii) a broad feature centred on 350 mT from magnetically interacting ions, probably also Fe^{3+}, (iii) a sextet component with peak separation ~9.5 mT centred on 350 mT from Mn (^{55}Mn, I=5/2), and (iv) a narrow feature centred on 350 mT from free radical defect centres in the mineral structure. Similar features have been reported in previous studies of kaolin samples (*e.g.* Goodman & Hall 1994), and are discussed individually below.

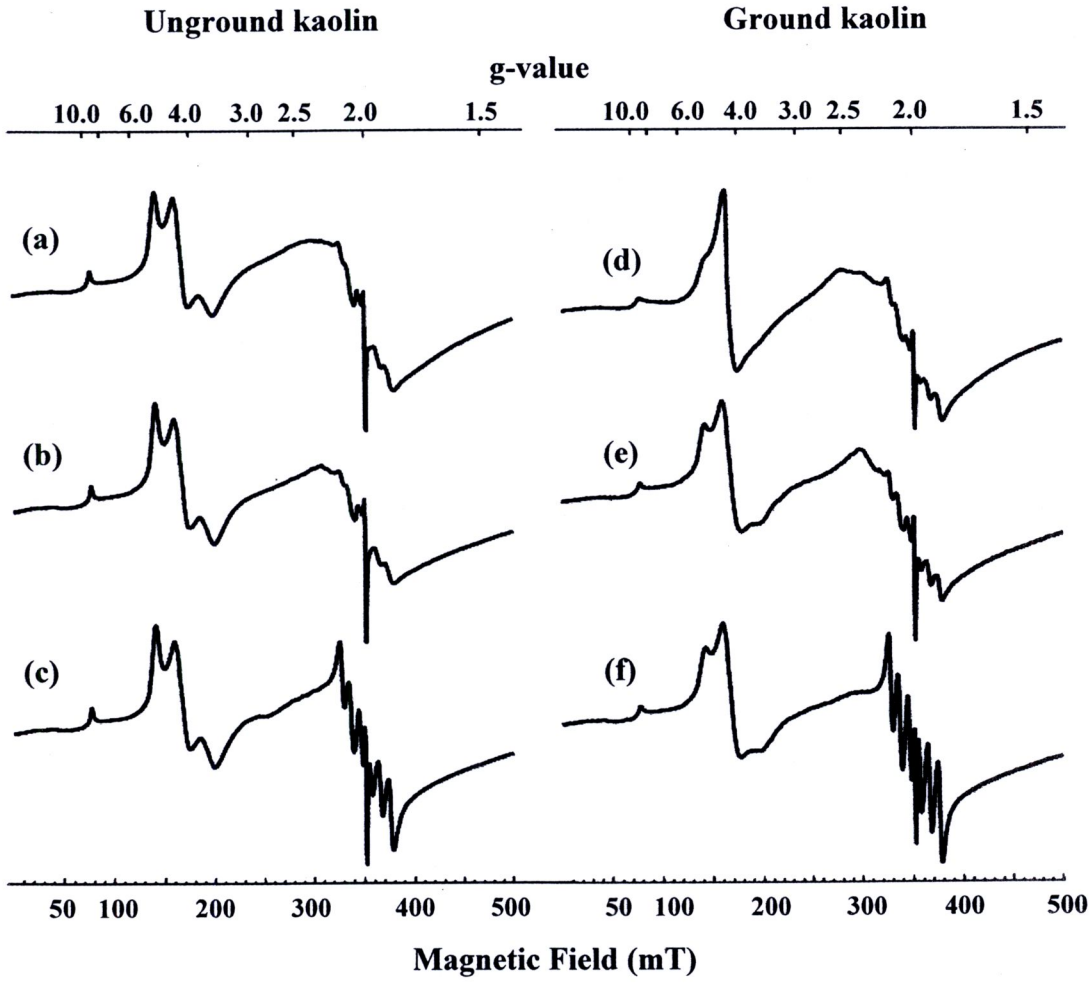

Figure 4.6 Wide scan EPR spectra of unground (a, b, c) and ground (d, e, f) Ranong kaolin samples without acid treatment (a, d) and after heating at 90°C for 4 h with 2 M H_2SO_4 and (b, e), or 0.7 M $H_2C_2O_4$ (c, f)

Low field signals in the range 50-250 mT are common features in the EPR spectra of kaolinites, and those in Figure 4.6 have been shown to correspond to Fe^{3+} in sites which experience two different types of structural distortion (Mestdagh, et al. 1980; Gaite, et al. 1997). As demonstrated by Balan et al. (1999) these low field features all correspond to substitution of Fe^{3+} for Al in octahedral sites within the kaolinite structure. The signal designated $Fe_{(I)}$ by Balan, et al. (1999), which corresponds to the central feature at 163 mT, results from the presence of a random distribution of vacant sites in adjacent layers in the structure. The remaining peaks in Figure 4.6 are all derived from the signal designated $Fe_{(II)}$ by Balan, et al. (1999), and correspond to Fe^{3+} in a well-ordered crystalline phase with ordered octahedral vacancies in its structure.

Physical treatment of the kaolin only affected the low field signals arising from Fe^{3+}; there was a decrease in the signals associated with $Fe_{(II)}$ and an increase in that associated with $Fe_{(I)}$ (Figure 4.6(d)). There was, however, little further change in these signals when the ground samples were extracted with sulfuric or oxalic acids (Figure 4.6(e,f)). In contrast to the low field Fe^{3+} signals, the Mn signal showed little change as a result of grinding alone, but its shape was modified by acid treatment. This resulted in a sharpening, but little change in the separation, of the Mn lines, and the effect was greater with the ground than with the unground kaolin; it was also much more pronounced with oxalic than with sulfuric acid treatment (Figure 4.6 (e,f)).

The free radical signal in the original kaolin is shown in Figure 4.7(a,b). The main feature is highly anisotropic with $g_{//} \sim 2.050$ and $g_{\perp} \sim 2.008$, and is similar to the A-centre described by Angel *et al.* (1974). It corresponds to electron holes trapped on oxygen atoms (Cuttler, 1981), and has been associated with radiation-induced defects in natural kaolinites (Clozel *et al.*, 1994). The $g_{\perp}$ region, however, clearly contains more than one feature, and is consistent with the Q-band EPR results of Clozel *et al.* (1994), who described the presence of three distinct free radical centres in kaolinite that had been subjected to γ-irradiation. Furthermore several (at least six) peaks are evident between the $g_{//}$ and $g_{\perp}$ features of the 2nd derivative spectrum and correspond to hyperfine structure from a radical centre involving interaction of unpaired electrons with ^{27}Al (I = 5/2) nuclei. This is consistent with the B-centre described by Clozel *et al.* (1995) as corresponding to O^- centre linking two Al atoms in octahedral sites, though

these authors were not able to determine whether this was at a surface position, or associated with an O atom linking the octahedral and tetrahedral sheets. It should also be noted that the present results cannot distinguish between a B-centre and one with a single ^{27}Al nucleus interacting with the unpaired electron.

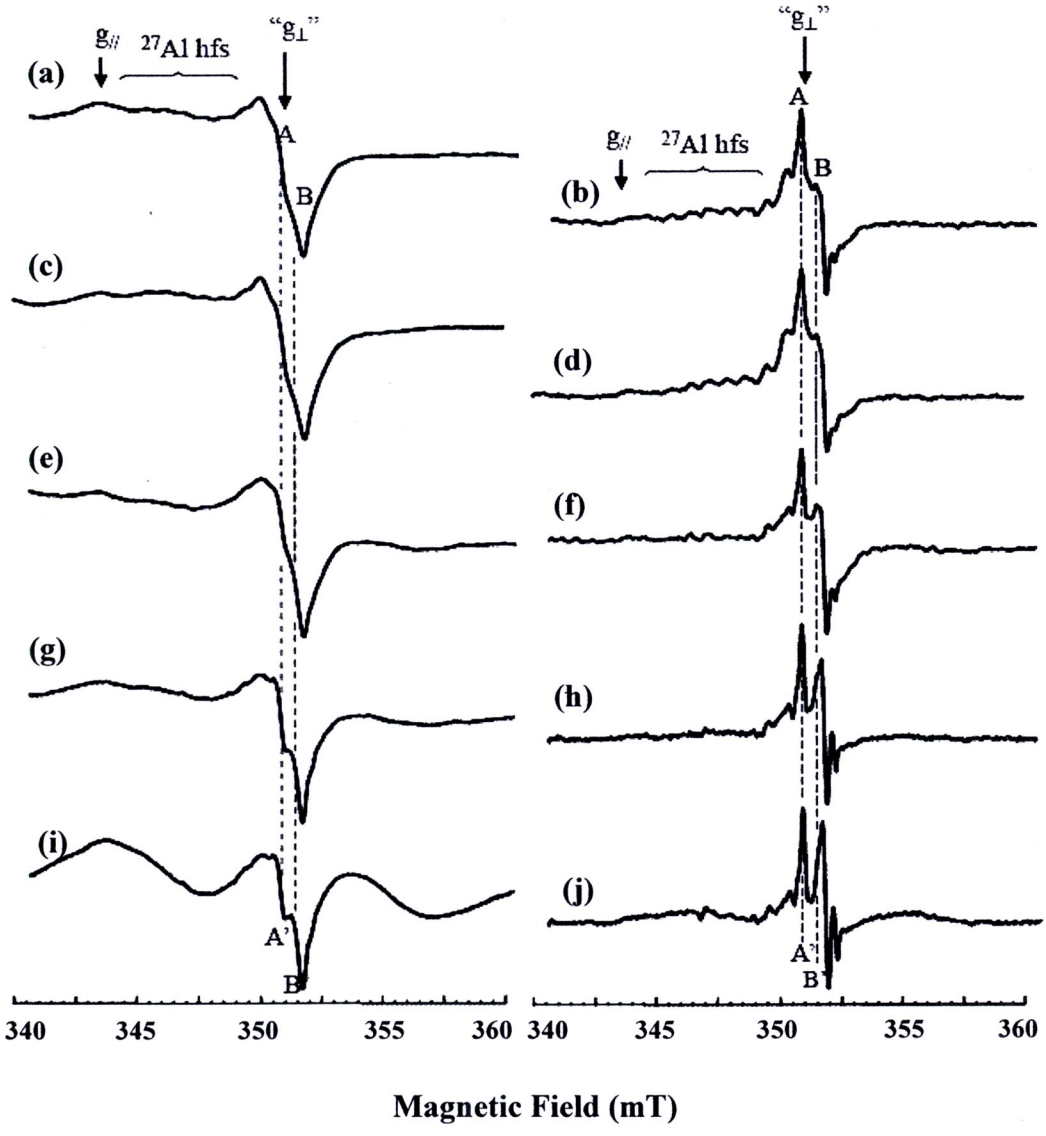

Figure 4.7 Expansion of the free radical region of the EPR spectra from the Ranong kaolin before (a,b) and after treatment with 2 M H_2SO_4 for 4 h (c,d) or grinding for 1 h in a ball mill (e,f),and after subsequent treatments of the ground sample with 2 M H_2SO_4 (g,h) and 0.7 M $H_2C_2O_4$ (i,j) for 4 h.

There was little influence of sulfuric acid extraction on the A-centre free radical signal, but there was an improvement in the resolution of the ^{27}Al hyperfine structure associated with the B-centre (Figure 4.7(c,d)). Since the most likely effect of the acid treatments is removal of surface adsorbed species, this result suggests that the B-centre is associated (at least partially) with a surface O atom on the octahedral sheet. Furthermore, the absence of any ^{1}H hyperfine structure indicates that this oxygen is not protonated.

Grinding resulted in a loss of the ^{27}Al hyperfine structure from the B-centre, although the signal from the A-centre was little changed, either by grinding alone, or subsequent acid treatment (Figure 4.7(g-j)). However, as seen by the variations in features labeled A and B in the $g_{\perp}$ region of the 2nd derivative recording (Figure 4.7) and Figure 4.8, the combined treatments resulted in a change in the relative amounts of the components that contributed to this absorption. However, at least one of these components probably corresponds to a defect centre in quartz for which radiation-induced defects are well-known (*e.g.* Weeks, 1956).

When the treated kaolin samples were resuspended in either sulfuric or oxalic acid at different pH values, there was little change in the low field Fe^{3+} signals. The widths of the Mn peaks, however, decreased with increasing pH, but the effect was far more pronounced with oxalic acid than with sulfuric acid (Figure 4.9). In the sample treated with sulfuric acid at pH 3.5, a new feature with $g \sim 2.5$ was also generated. This was reproduced in replicate experiments, and it thus corresponds to a genuine product. However, its interpretation is unclear, although Golding et al (1977) have shown that under certain conditions, Fe(III) can produce an isotropic spectrum with $g = 3.3$.

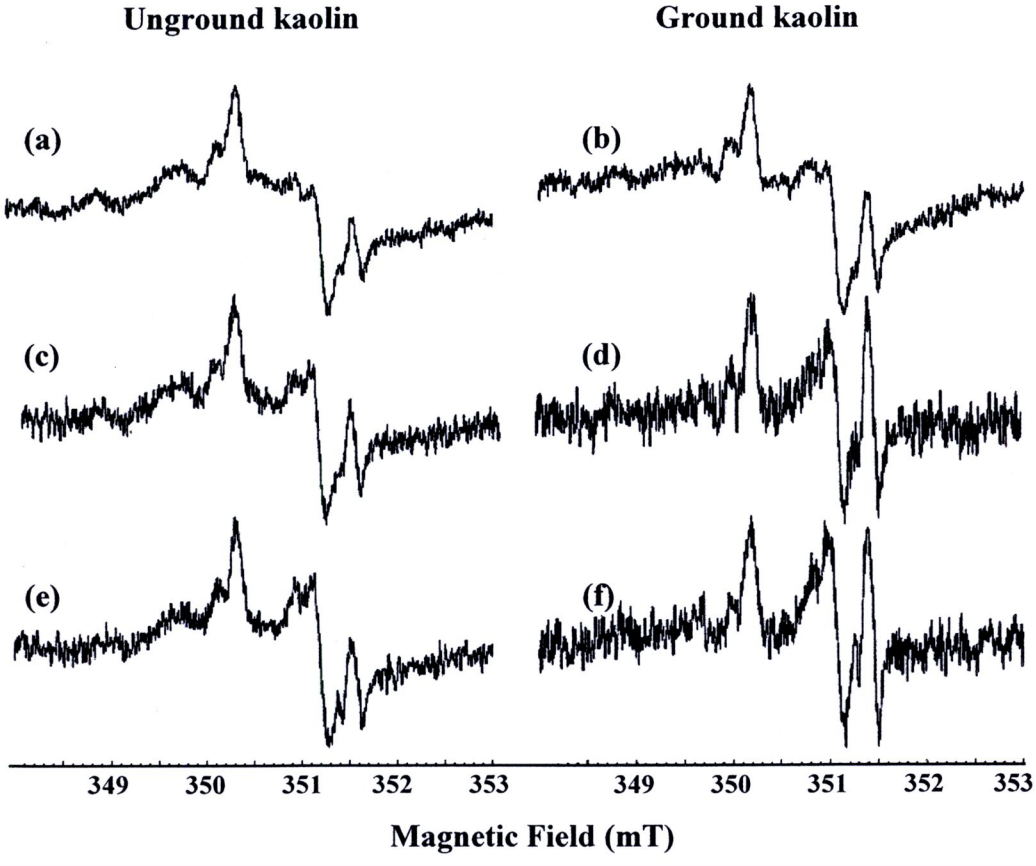

Figure 4.8 2nd derivative recordings showing the effects of grinding and acid treatments on the $g_{\perp}$ region of the free radical EPR free radical signal from Ranong kaolin (a) untreated, (c) after heating at 90°C for 4 h with 2 M H_2SO_4, (e) after heating at 90°C for 4 h with 0.7 $H_2C_2O_4$, and after grinding for 1 h in a ball mill (b),then subsequent treatments with 2 M H_2SO_4 (d) and 0.7 M $H_2C_2O_4$ (f) for 4 h.

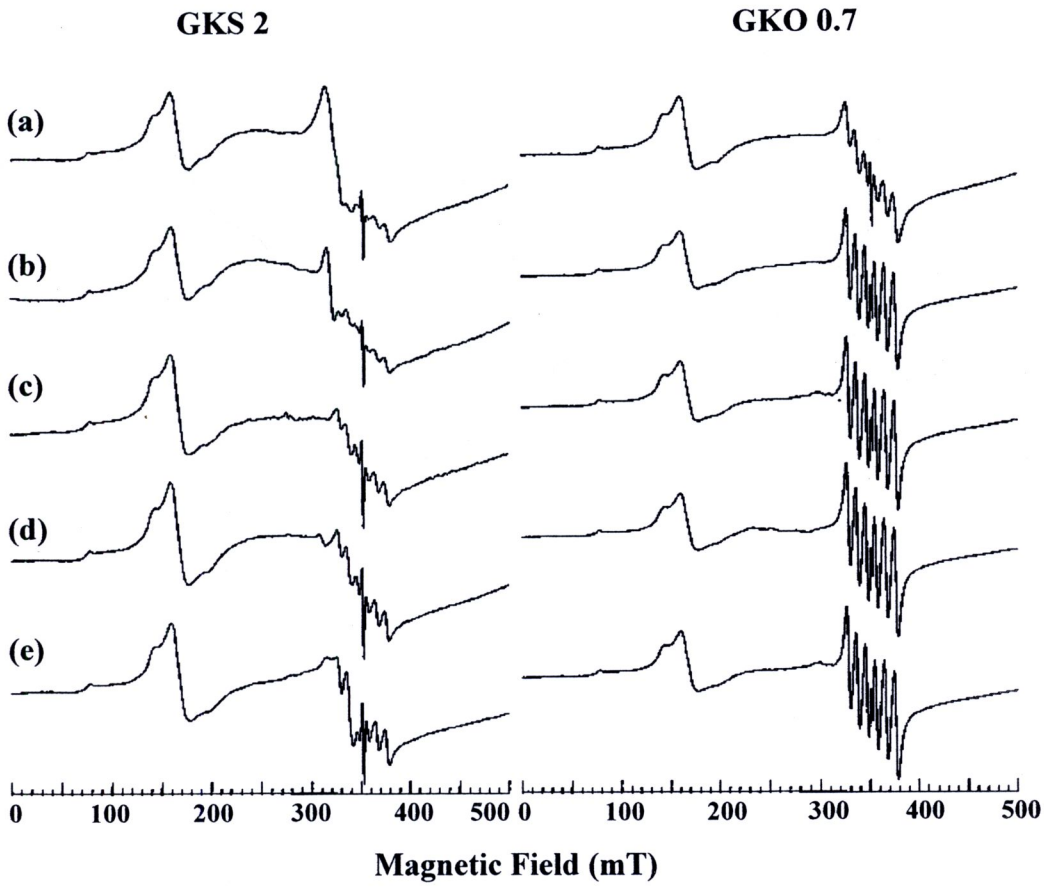

Figure 4.9 Effect of adjusting the surface pH on the Mn EPR signal from Ranong kaolin that had been ground for 1 h in a ball mill and extracted with either 2 M H_2SO_4 or 0.7 M $H_2C_2O_4$, (a) pH 2.0, (b) pH 3.0, (c) pH 3.5 (d) pH 4.0, and (e) pH 5.0.

4.1.5 Scanning electron microscopy (SEM) studies

Results from SEM/EDS studies of the Ranong kaolin and its modified products are shown in Figure 4.10. The original clay sample, NK, shows the presence of both platy and tubular shapes that are characteristic of kaolinite and halloysite, respectively. Chemical analysis of sample surfaces performed using EDX indicate that Si, Al, O are the major elements, and K and Fe are minor components, as was found with the XRF analyses of the bulk samples. However, these structures were largely destroyed by grinding (Figure 4.11(a)). Hot acid treatments of the ground sample then resulted in the formation of products with globular morphology and smaller particle size (Figure

4.11(b,c)), consistent with the increased surface area (**Section 4.1.6**). Furthermore, acid treatment of the ground samples resulted in an appreciable decrease in the Al content.

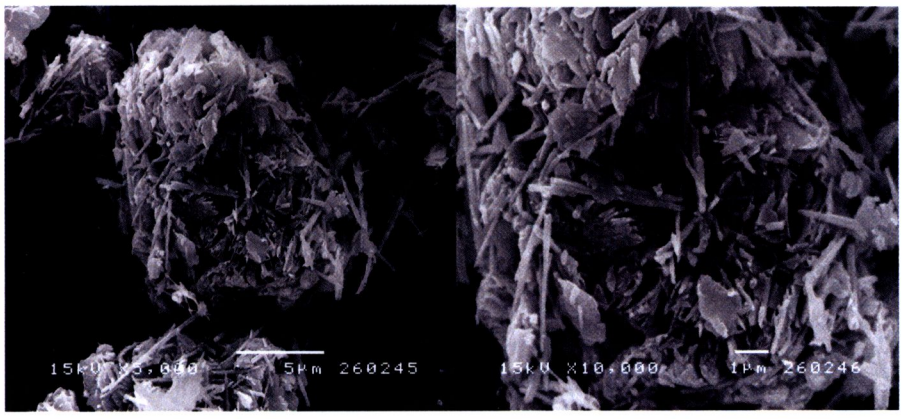

SEM micrographs of natural Ranong kaolin

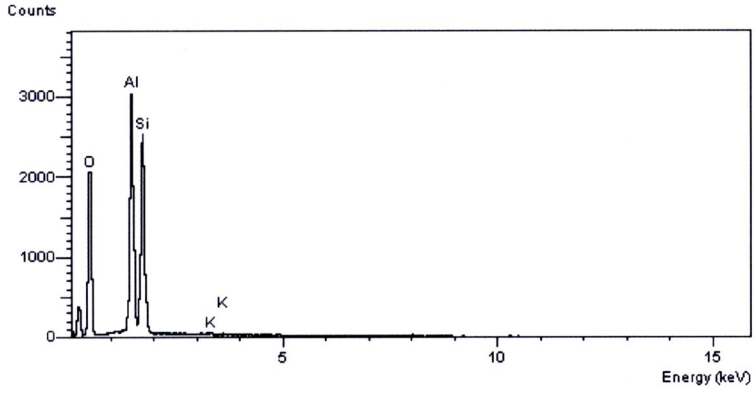

EDX spectrum

Figure 4.10 SEM micrographs of natural Ranong kaolin sample magnified x5,000, x10,000 , and representative EDX spectrum

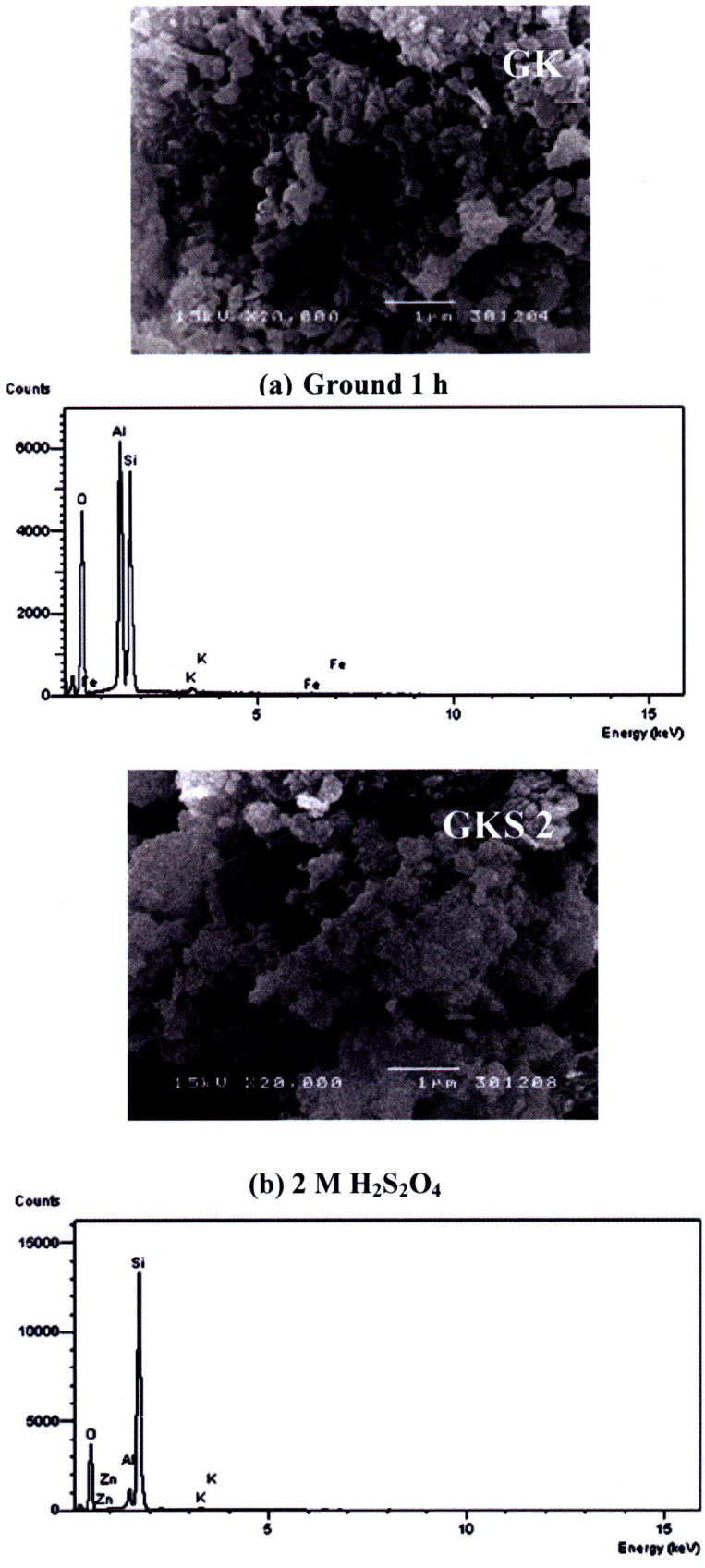

Figure 4.11 SEM micrographs and representative EDX spectra from small areas on the surface of Ranong kaolin samples (a) ground 1 h, then treated with (b) 2 M H_2SO_4, and (c) 0.7 M $H_2C_2O_4$ for 4 h at 90 °C.

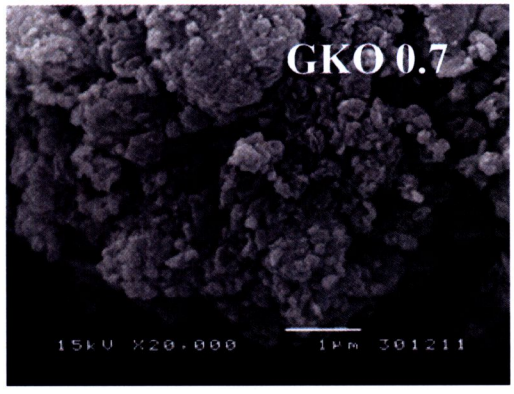

(c) 0.7 M $H_2C_2O_4$

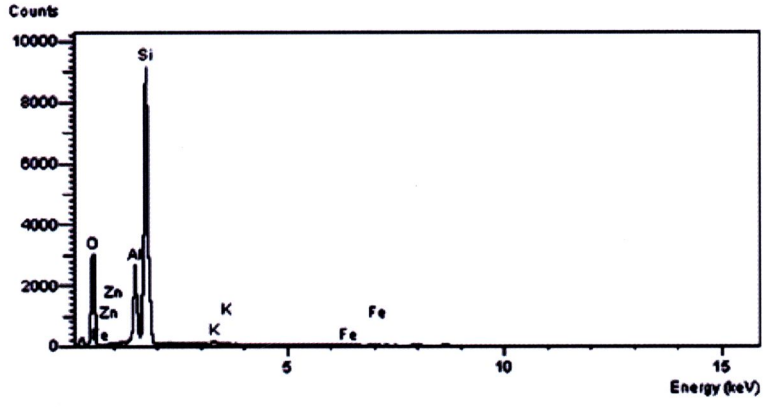

Figure 4.11 (con't)

4.1.6 Determination of surface and textural properties

The textural properties; specific surface areas (S_{BET}), total pore volumes (V_P),average pore diameter ($\bar{r}$) of Ranong kaolin before and after modification are summarized in Table 4.4, and the pore size distributions (PSD) are shown in Figure 4.12

Table 4.4 Specific surface area (S_{BET}), total pore volume (V_p), mesopore–micropore volumes (V_{me}, V_{mi}), average pore diameter ($\bar{r}$), and decolorisation capacities (DC) of some kaolin samples and a commercial bleaching clay (CBC).

Sample	S_{BET} (m^2/g)	V_p (cm^3/g)	V_{me} (cm^3/g)	V_{mi} (cm^3/g)	$\bar{r}$ (nm)	DC (%)
NK	13.1	.06	.06	.00	19.7	-
GK	33.1	.14	.14	.00	16.4	-
UGKS 2	46.0	.10	.10	.00	8.3	43.30
UGKS 3.7	57.7	.12	.12	.00	8.5	54.14
GKS 1.7	230.2	.51	.48	.03	8.8	71.94
GKS 2	243.6	.43	.40	.03	7.0	79.63
GKS 2.5	216.8	.47	.44	.02	8.6	75.73
GKS 3	214.1	.51	.49	.02	9.4	71.20
GKS 3.7	201.6	.49	.47	.02	9.7	65.20
GKO 0.5	195.6	.32	.28	.03	6.6	72.79
GKO 0.7	225.8	.37	.34	.03	5.6	78.40
GKO 0.9	228.5	.32	.29	.03	6.5	75.40
CBC	153.2	.29	.29	.00	7.5	81.93

The specific surface area (S_{BET}) and total pore volume (V_P) of natural Ranong kaolin are 13.1 m^2/g and 0.06 cm^3/g, respectively. After chemical treatment, UGKS 2 and UGKS 3.7 showed respectively 3.5-fold and 4.3-fold increases in S_{BET} and 1.5-fold and 1.9-fold increases in V_P, indicating that some acid attack on the kaolin structure occurred. Grinding resulted in an almost 3-fold increase in the value of S_{BET} and a doubling of the V_P value. Major changes were observed, however, on subsequent acid leaching of the ground sample, when a further 6 to7-fold increase in S_{BET} and a further 2.5- to 3.7-fold increase in V_P were observed. Thus the combination of physical and chemical treatments produced ~18.5-fold and ~7.9-fold increases in S_{BET} and V_P, respectively.

The mesopore volume (V_{me}) increased 2-fold after grinding and ~4.4- to 6.2-fold after the combined physical and chemical treatments. The average pore diameter ($\bar{r}$), considered to be the more important property for pigment adsorption (Sabah 2007; Sabah et al. 2007; Hulya et al. 2007 and Temuujin et al. 2006) was ~ 5.6-7.0 nm. Much smaller changes in these properties were observed with chemical treatment of unground kaolin samples. These results are comparable with those observed by other workers for modified kaolins. For example Temuujin et al. (2006) found that the S_{BET} of their

kaolin increased from ~15 m^2g^{-1} to ~300 m^2g^{-1} as a result of mechanical activation followed by acid leaching; in addition, V_P increases of 0.28-0.31cm^3g^{-1} were observed.

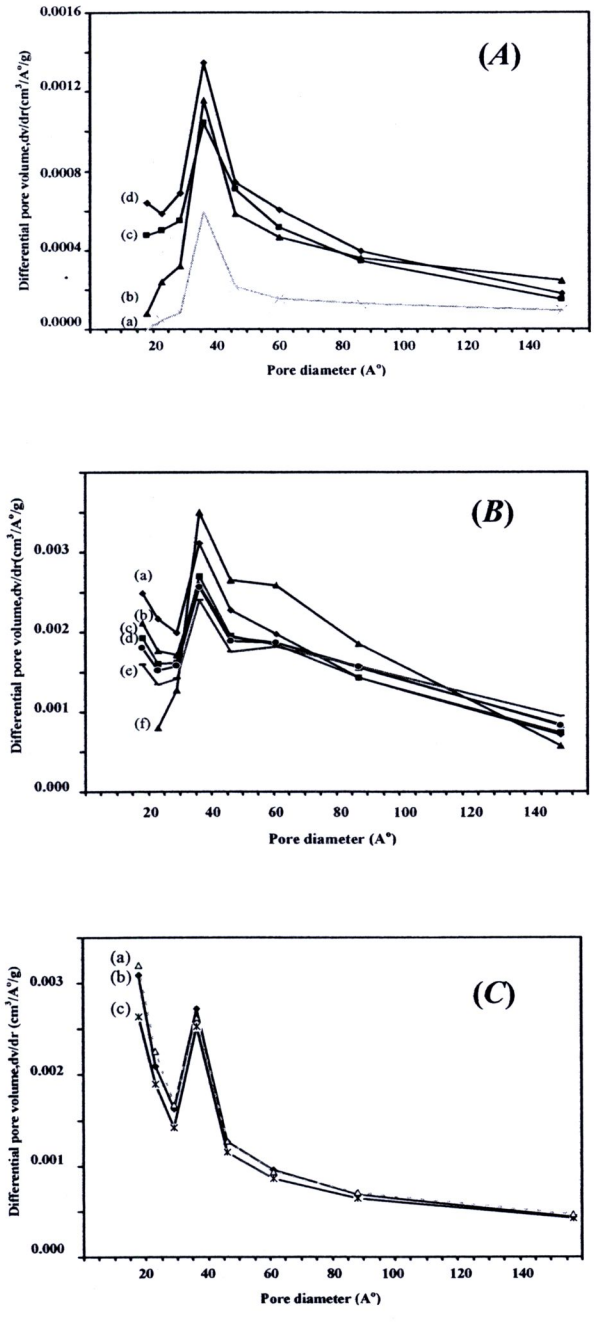

Figure 4.12 Pore size distribution (PSD) of (*A*) (a) natural kaolin (NK) (b) ground Kaolin (GK), NK after leaching with 2 M H_2SO_4 (c) and 3.7 M H_2SO_4(d) (*B*) GK after leaching with various concentrations of H_2SO_4 (a) 2 M (b) 2.5 M (c) 1.7 M (d) 3.0 M (e) 3.7 M, and (f) a commercial bleaching clay (CBC) (*C*) GK after leaching with various concentrations of $H_2C_2O_4$ (a) 0.5 M (b) 0.7 M, and (c) 0.9 M.

The pore size distribution (PSD) curves of natural kaolin, ground kaolin, modified kaolin samples and commercial bleaching clay are shown in Figure 4.12 (*A-C*). It is seen that grinding kaolin increased the proportion of pores in the ~ 3.0-4.5 nm range and that there was a further increase in the proportion of pores in this region after acid treatment (Figure 4.12 (*A*) and (B)). The pore size distribution plots indicate that the *dv/dr* ratio (ratio of change in volume relative to the radius) increased as a result of grinding followed by leaching with 2M H_2SO_4 (GKS 2) Figure 4.12(*B*) compared to the natural sample and acid treatment products (UGKS 2 and 3.7) (Figure 4.12 (*A*) and (*B*)). The GKS 2 sample exhibited a maximum in differential pore volumes at ~3.6 nm and was similar to the CBC; GKS 2 and GKS 2.5 also had sharp peaks at a radius of 3.6 nm (Figure 4.12 (*B*)).

4.1.7 Point of Zero Charge

Plots of the variation of net surface charge with pH are shown in Figure 4.13 for the Ranong kaolin after grinding and extraction with sulfuric or oxalic acids. These results show Pzc values of ~3.5 and ~3.7, respectively for the products after treatment with sulfuric and oxalic acids.

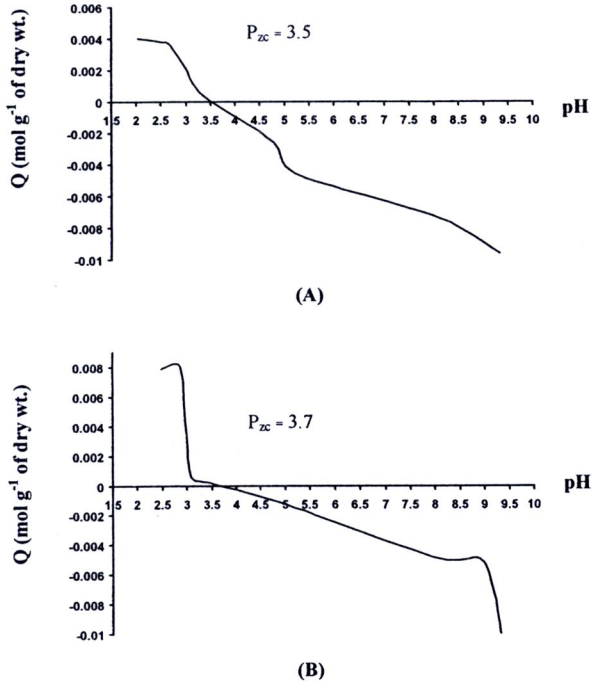

Figure 4.13 Determination of the point of zero charge (P_{ZC}) for modified kaolin samples (A) GKS 2 and (B) GKO 0.7.

4.2 Adsorption (Bleaching) studies

4.2.1 Influence of contact time

Bleaching of crude rice bran oil is more difficult than most other vegetable oils, because of the presence of high chlorophyll contents, products of oxidized tocopherols, and metallic salts of fatty acids (Ghosh, 2007).

The general procedure for bleaching oils is to apply a temperature of 80-120°C for 15-30 minutes under vacuum in the presence of bleaching earths (Baranowsky, et al., 2001). The dosage of bleaching earths can vary between 0.5-2% on a weight basis depending on the oil type (Valenzuela Diaz and Souza Santos, 2001). In this study, the bleaching experiments were performed at 90±2°C to avoid oxidation problems experienced at high temperature, such as the production of oxidation products and Millard browning products (Proctor and Toro-Vazquez, 1996; Kochhar, 2001). However, in order to study the effect of contact time, the bleaching experiments were performed for 15, 30, 60 and 120 minutes using UGKS 2 and UGKS 3.7. The results are illustrated in Figure 4.14.

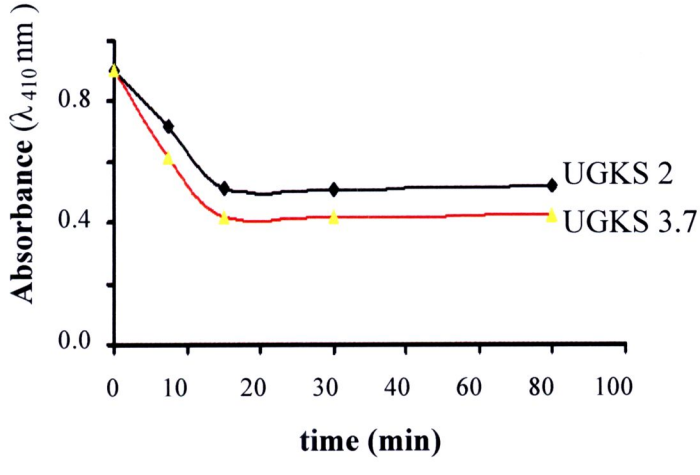

Figure 4.14 Influence of contact time on bleaching of rice bran oil using kaolins treated with 2 M and 3.7 M H_2SO_4 (UGKS 2 and UGKS 3.7, respectively). The dosage, weight ratio of clay and oil was 2% (w/w).

From the results of the contact time study, it was revealed that the rate of adsorption increased linearly with time during the first period of adsorption (~30 min), but there was then no subsequent change with longer contact times. Thus, a contact time of 30 min is adequate for the bleaching process.

4.2.2 Adsorption efficiency

The decolorisation capacities (%) of the various modified kaolin samples are shown in Table 4.4. These increased with increasing acid concentration, but the values for unground kaolin samples were much lower than for ground kaolin with the same acid concentration (*e.g.* ~43% for UGKS 2 (unground) and ~80% for GKS 2(ground)). For acid activated ground samples, the optimum sulfuric acid concentration was 2M, and that for oxalic acid was 0.7 M; higher acid concentrations resulted in lower decolorisation capacities (Table 4.5). This has been interpreted as being due to the collapse of the clay lattice structure in the presence of excess acid (Kheok and Lim, 1982; Woumfo et al., 2007). Tong et al., (2008) has also reported that excessive acid strengths led to decreases in specific surface area, and total pore volume.

Table 4.5 Decolorisation capacity (%) of modified kaolin

Sample (2%w/w)	Decolorisation capacity (%)
Acid activation	
UGKS 2	43.3 ± 0.02
UGKS 3	52.7 ± 0.04
UGKS 3.7	54.1 ± 0.03
UGKS 5	59.8 ± 0.02
Grinding and acid activation	
Sulfuric acid leaching	
GKS 1.7	71.9 ± 0.02
GKS 2	79.6 ± 0.03
GKS 2.3	78.9 ± 0.03
GKS 2.6	75.7 ± 0.02
GKS 3	71.2 ± 0.05
GKS 3.7	65.2 ± 0.01
Oxalic acid leaching	
GKO 0.5	72.8 ± 0.03
GKO 0.7	78.4 ± 0.04
GKO 0.9	75.4 ± 0.03
CBC (commercial bleaching clay)	81.9 ± 0.03

4.2.3 Influence of surface modification by variation of the pH of kaolin suspensions

The influence of the pH of the suspension from which the kaolin sample was prepared on the efficiency of decolorisation of rice bran oil is illustrated in Table 4.6.

Table 4.6 Decolorisation capacity (%) at various pH of clay suspension

pH	Decolorisation capacity (%)	
	GKS 2	GKO 0.7
2.0	80.88±0.03	79.79±0.02
2.5	80.64±0.01	79.59±0.01
3.0	80.51±0.03	78.69±0.02
3.5	78.95±0.02	78.30±0.02

The highest efficiency was observed for pH values of 2.0-3.0; lower values were observed for pH ≥3.0. Similar trends were observed for sulfuric acid and oxalic acid treatments of ground kaolin, and the results thus show that the pH of the clay surface affects the adsorption process, and plays an important role in the bleaching efficiency of kaolin. The P_{ZC} of the modified kaolin were ~3.5 and ~4.7 for GKS 2 and GKO 0.7, respectively, and hence increased adsorption below these values indicates interactions with anionic or negatively-charged regions of polar material, such as chlorophyll-a, which is a major pigment in rice bran oil. These results are consistent with reports by other workers on the effects of pH on clay adsorption properties. For example, Velde (1992) found that the highest adsorption of organic molecules by clays occurred in the pH range 2-4, and Girgis (2005) reported that the optimum pH for the removal of color from vegetable oil by bleaching earth was in the range 2.5-3.0.

4.3 Characterisation of the interaction between pigments in rice bran oil and modified kaolins

The modified kaolin changed color from pale yellow to green as a result of adsorption of pigments during bleaching rice bran oil; it was suspected that these pigments could be chlorophyll or its derivative, pheophytin, since these are major pigments in rice bran oil. After the bleaching process, the adsorbent was washed several times with stirring

and soaked with hexane overnight, in order to dissolve any rice bran oil remaining in clay sample, but the clay remained green. Thus there is a strong interaction between the pigment and the modified kaolin. In order to gain additional understanding of the chemical/physical nature of the adsorption process, further investigations were performed to identify changes induced in the most of the modified kaolin samples as a result of their use in the bleaching process and removal of any associated oil. These involved desorption studies supplemented by diffuse reflection Fourier transform infrared (DRIFT), electron paramagnetic resonance (EPR) spectroscopy and scanning electron microscopy (SEM)

(a) (b)

Figure 4.15 Photographs of GKS 2 (a) before, and (b) after use for rice bran oil bleaching followed by overnight extraction with hexane.

4.3.1 Diffuse reflectance infrared Fourier transform (DRIFT)

DRIFT spectra of degummed and neutralized rice bran oil and modified kaolin, GKO 0.7 and GKS 2 before and after use for rice bran oil bleaching and removal of any associated oil are presented in Figures 4.16.

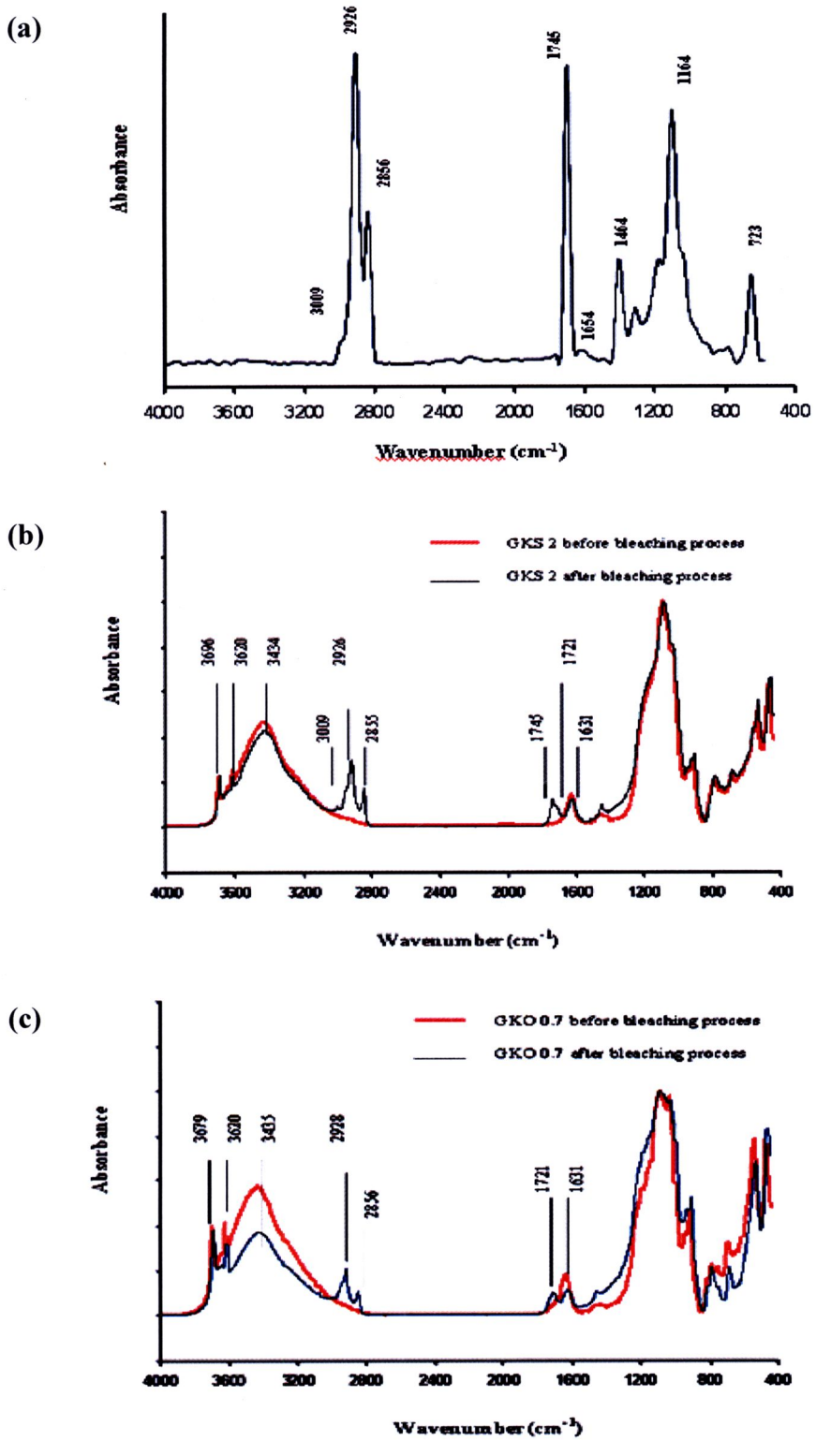

Figure 4.16 DRIFT spectra of (a) degummed and neutralized rice bran oil (b) modified kaolin GKS 2 and (c) modified kaolin GKO 0.7 before and after adsorption of colored material from rice bran oil.

The spectra of degummed and neutralized rice bran oil show bands around 3009, 2926, and 2856 cm^{-1} that are assigned respectively to the C-H stretching vibrations of the *cis*-double bond (=CH), symmetric and asymmetric stretching vibrations of the aliphatic CH_2 group in organic compounds. The 1745 cm^{-1} band is attributed to the ester carbonyl function group. These bands are attributed to the chlorophyll functional group, because chlorophyll and its derivatives are major pigments in crude rice bran oil, (see Figure 4.17).

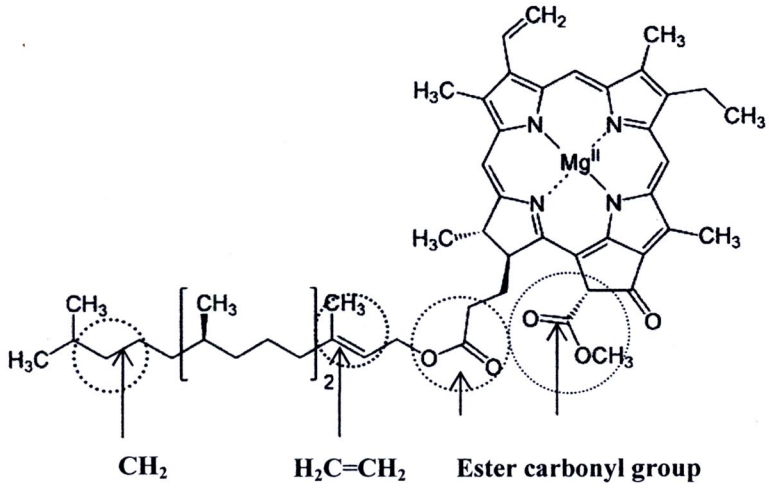

Figure 4.17 Structure of chlorophyll-a molecule

The modified GKS 2 and GKO 0.7 after use for rice bran oil bleaching was washed with hexane with stirring and soaked over night in order to dissolve any remaining rice bran oil, but the clay remained green. Thus the green pigment was adsorbed on the clay. DRIFT spectroscopy was used to investigate the interaction between pigment and clay surface (Figure 4.16). Pigment adsorption resulted in the appearance of new bands at 2855 cm^{-1}, 2926 cm^{-1}, and 3009 cm^{-1}; these correspond to the symmetric, asymmetric – CH_2 stretching vibrations of hydrocarbon chains, and the C-H stretching vibration of the *cis*-double bond, respectively. The sharp band at ~2926 cm^{-1} may correspond to phytol in adsorbed chlorophyll (pheophytin), since this gives a strong C-H stretching band (Weigl and Livingston, 1953; Holt and Jacobs, 1955). Another band at ~1745 cm^{-1} is consistent with ester carbonyl groups of chlorophyll (Weigl and Livingston, 1953; Holt and Jacobs, 1955). However, in this study spectral changes were also observed in the C=O region (~1745 cm^{-1}), and the appearance of a shoulder at ~1721 cm^{-1} that may be

attributed to the interaction of acidic sites on the kaolin surface and ester carbonyl groups of chlorophyll.

Thus this result suggests chemical interactions occur between the adsorbent and pigments in rice bran oil, probably involving interactions of the ester carbonyl group of chlorophyll with acidic sites on the clay surface. Sabah (2007) has reported that chlorophyll adsorption on acid activated sepiolite involves active sites on the mineral surface, whereas Mehraban and Farzaneh (Mehraban and Farzaneh, 2006) reported that chlorophyll adsorption by the zeolite MCM-41 involves electrostatic interactions between chlorophyll and surface silanol groups. Our studies indicate that the interaction between pigments and acidic sites on the modified clay involve a combination of electrostatic interactions and chemical bonds.

4.3.2 EPR spectroscopy

EPR spectra of the Ranong kaolin before and after its use for bleaching rice bran oil (Figure 4.18) showed no changes in the signal that is assigned to $Fe^{3}+$ in octahedral sites (Gaite, et al.,1997; Balan, et al.,1999), but there was considerable distortion of the Mn signal, which is thought to correspond to Mn^{4+} in tetrahedral sites (see **Section 4.8**). Thus it appears that the material adsorbed from the oil affects the tetrahedral surface, but has little effect on the octahedral surface. An alternative explanation of this observation is that there is some adsorption of Mn-containing material from the oil, and this interferes with the signal from Mn in the kaolinite structure. One possible source of the Mn could be chlorophyll, since some Mn^{2+} is associated with chlorophyll in plant leaves (Goodman and Newton, 2005). However, no Mn signal was observed in the EPR spectrum of the unbleached rice bran oil (spectrum not shown), so a change in the symmetry of the Mn-containing sites in the kaolinite structure is considered to be the more likely explanation for the changes in the kaolin EPR spectra resulting from pigment adsorption.

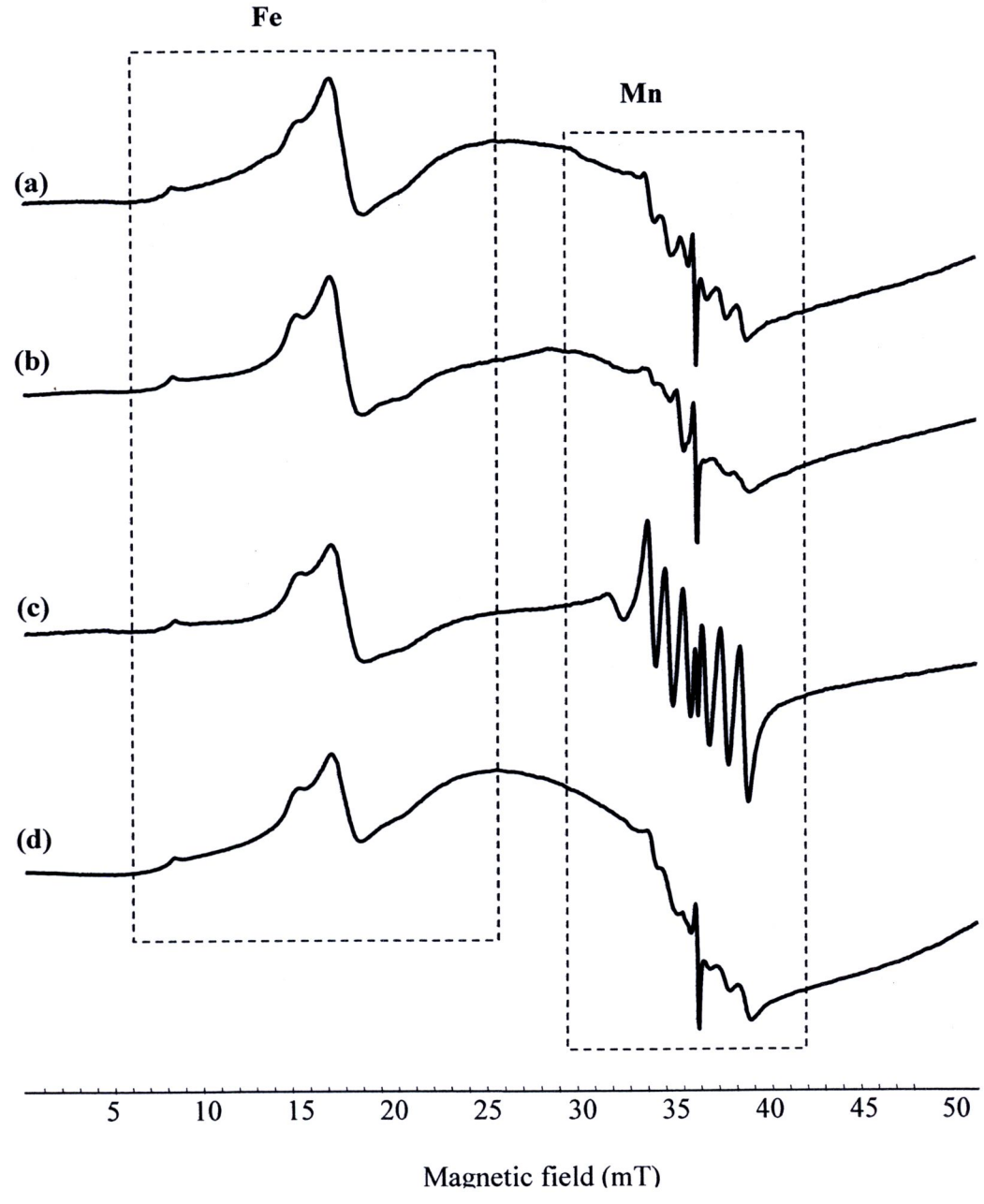

Figure 4.18 EPR spectra of kaolinite samples: GKS 2 (a) before and (b) after adsorption rice bran oil, GKO 0.7 (c) before and (d) after adsorption rice bran oil.

In addition to changes to the Mn signal, there is an increase in the broad background signal, and an increase in the free radical signal centred on g = 2.00 (~350 mT) after use of the kaolinite for bleaching the oil. The background signal corresponds to

magnetically-interacting ions, and is not definitive for any particular chemical species. However, in natural samples, it is generally associated with iron oxides (Goodman and Hall,1994), and could, therefore, be associated with the adsorption from the rice bran oil of ferritin (the main iron storage protein in plants), which can be associated with chloroplasts (Long et al., 2008) as well as mitochondria. Characterisation of the spectral properties of the free radical signal produced as a result of the sorption process is also difficult, because of its overlap with a free radical signal associated with defects in the mineral structure, but it appears to be a single peak resonance with line width around 0.5 – 0.6 mT. This is similar to the weak free radical seen in the unbleached oil (Figure 4.18(a)) and to the colored material (melanoidins) seen in many plant pigments, such as seed testa (Hepburn, et al., 1986). Hence this free radical probably corresponds to adsorption of similar material.

4.3.3 Scanning electron microscopy (SEM)

The morphology, texture and particle shape of modified kaolins before and after use for bleaching are illustrated in Figure 4.19. Before use for oil bleaching the modified kaolin, GKS 2, had a sponge-like appearance with numerous pores with distinct texture (Figure 4.19(a)); high porosity and pore connectivity are important adsorption properties of modified clays (Mokaya et al., 1993). The mineral morphology changed drastically after pigment adsorption and associated oil removal. Large pigment molecules were observed on the clay surface, and produced a thick cover over most of the pore cavities (Figure 4.19(b)).

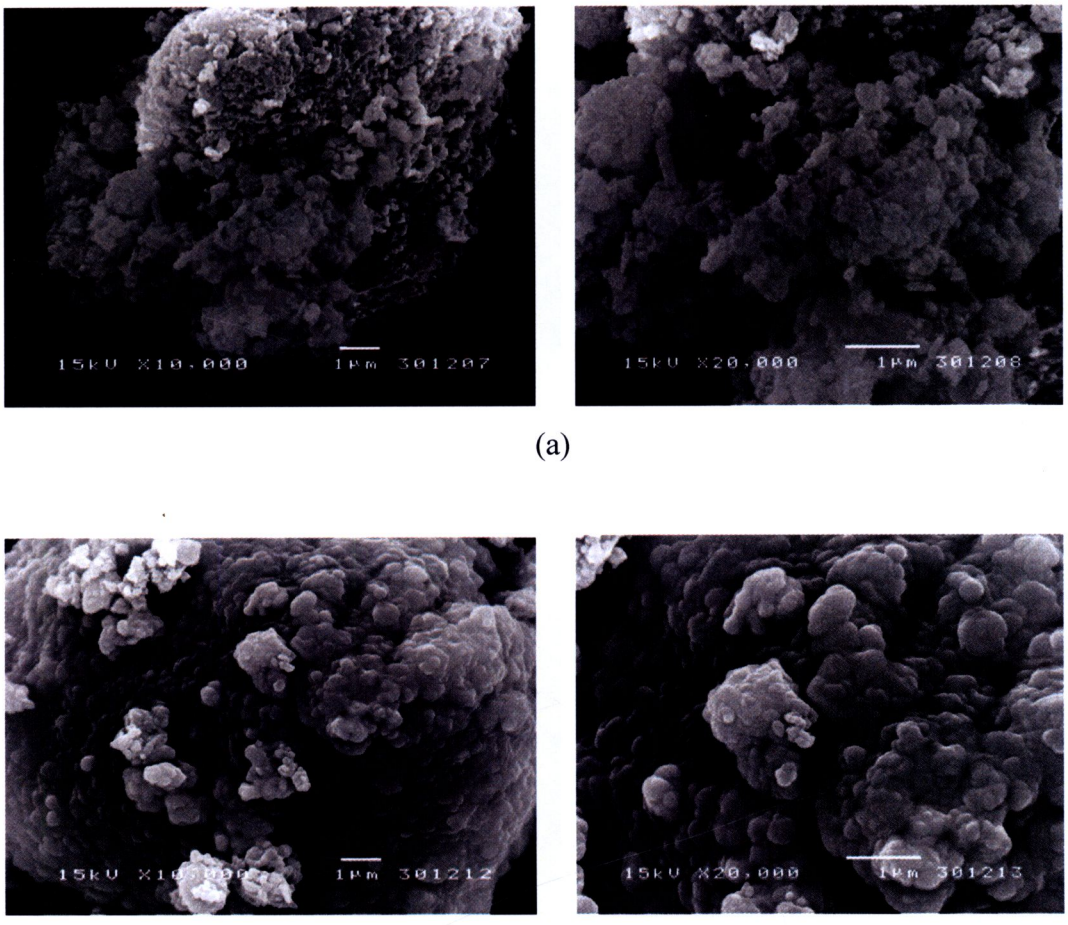

Figure 4.19 SEM micrographs of kaolin sample GKS 2 (a) before and (b) after use for adsorption of colored material from rice bran oil.

The scanning electron micrograph of GKO 0.6 (Figure 4.20 (a)) resembles that of GKS 2, but with fewer pores and smaller cavities. Adsorption of pigments by this clay sample was less efficient than with GKS 2, and fewer pigment molecules were observed on the clay surface after adsorption and oil removal. Some pore structures could still be observed indicating that pigment molecules were not able to penetrate these small cavities (Figure 4.20 (b)). Thus although the specific surface areas of the two modified clays were similar, the decolorisation capacity of the clay was influenced by the pore diameter of the modified structure.

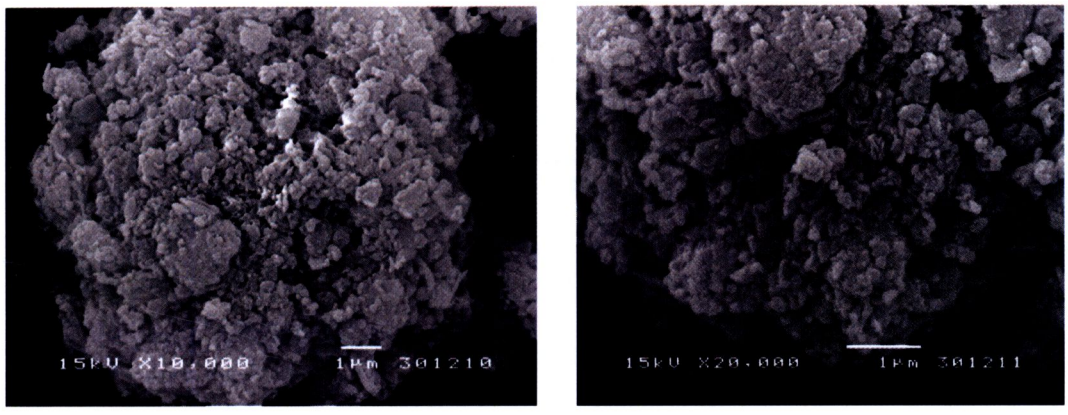

(a)

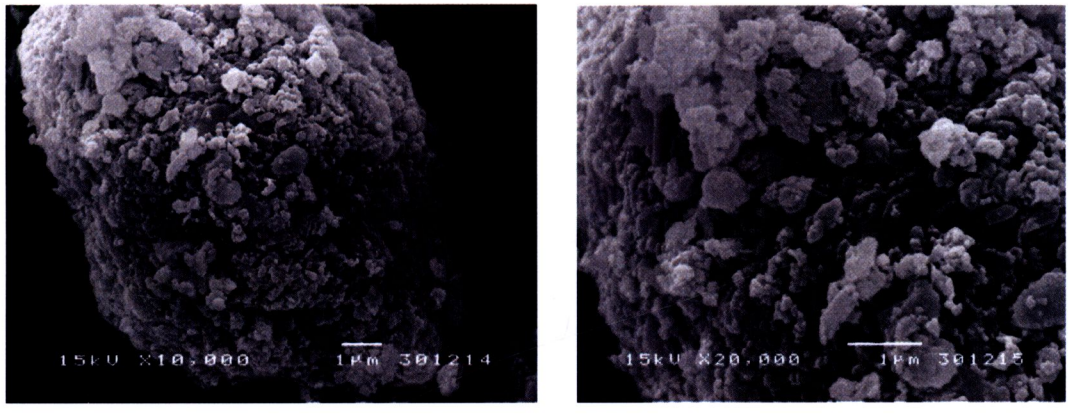

(b)

Figure 4.20 SEM micrographs of kaolin sample GKO 0.7 (a) before and (b) after use for adsorption of colored material from rice bran oil

4.3.4 Adsorption isotherm studies

In this work, the Freundlich and Langmuir isotherm models were used to study the adsorption process during rice bran oil bleaching. The results are shown Figures 4.21 (a-c) and Figure 4.22 (a-c).

The Freundlich adsorption isotherms were plotted for rice bran oil bleaching at various temperatures, and the values of log K_F and n were obtained from the graphs, where n is the slope and log K_F the y-axis intercept. The values of K_F and n for GKS 2 at 60, 75 and 90°C are summarized in Table 4.7, which also shows the related correlation coefficients (R^2 values). K_F increased in the order 60 < 75 < 90°C.

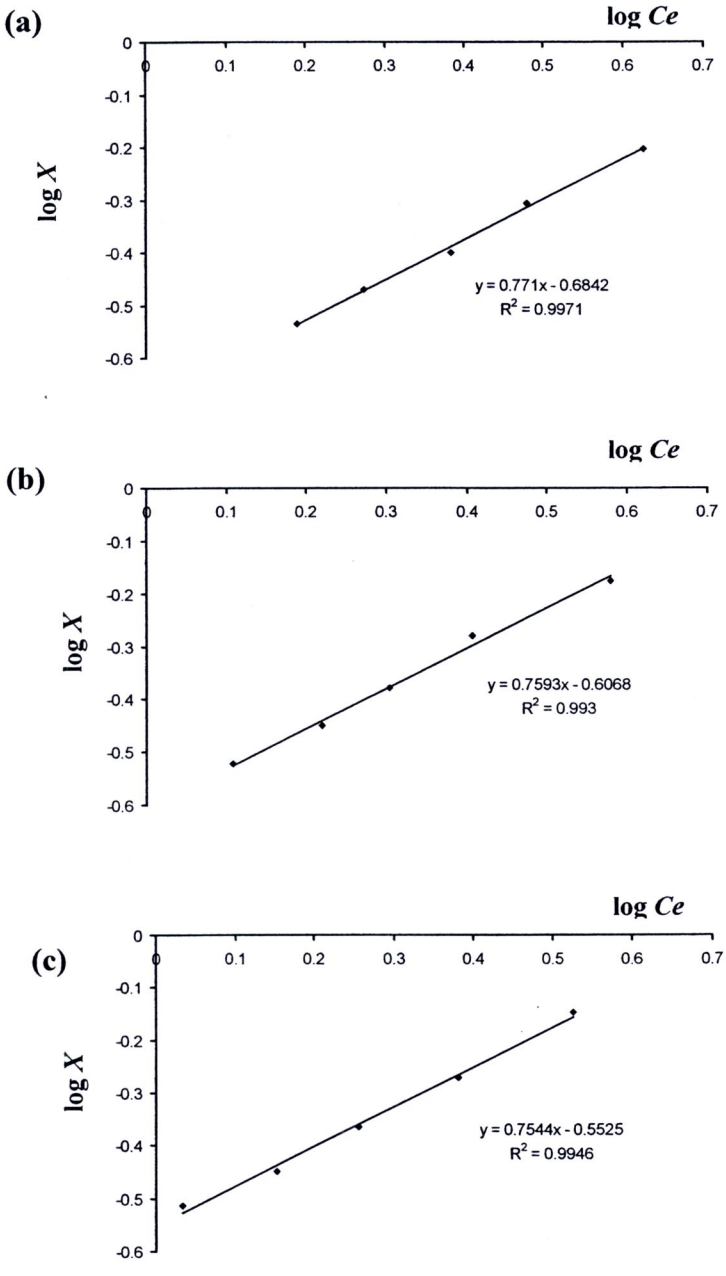

Figure 4.21 Freundlich isotherm in its linear form for rice bran oil bleaching by GKS 2 at (a) 60 °C , (b) 75 °C, and (c) 90 °C

As previously described, the constant K_F is an indicator of the adsorption capacity or decolorisation capacity of the adsorbent, whereas n is an indicator of the manner of adsorption. The larger the K_F value, the more effective the adsorbent for adsorption.

Thus in this bleaching process, the results show that the highest temperature is the most favourable condition.

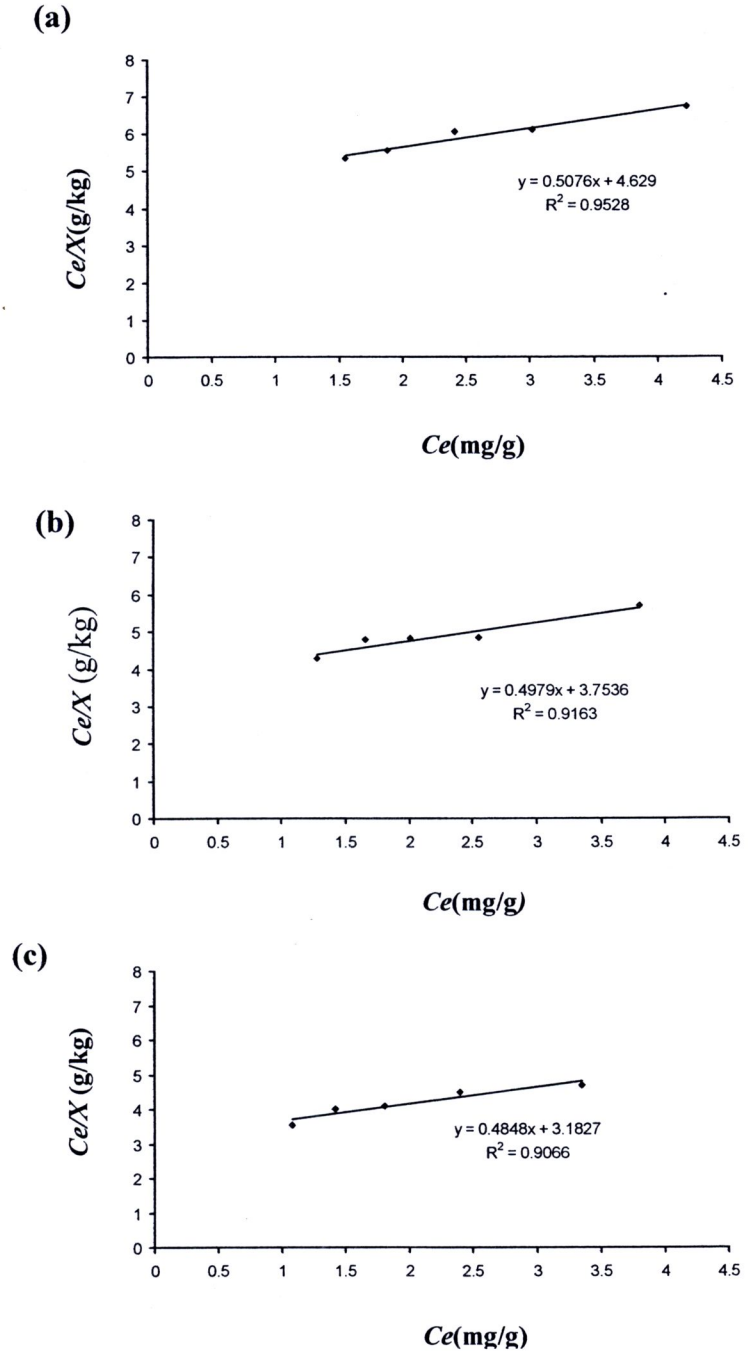

Figure 4.22 Plots of the Langmuir isotherm in its linear form for rice bran oil bleaching by GKS 2 at (a) 60 °C , (b) 75 °C, and (c) 90 °C

Table 4.7 Freundlich isotherm constants for the bleaching of rice bran oil using GKS 2 at various temperatures

Temperature (°C)	Freundlich constants		
	K_F	n	R^2
60	0.2069	1.2970	0.9971
75	0.2473	1.3170	0.9930
90	0.2802	1.3256	0.9946

The Langmuir adsorption isotherms were plotted for rice bran oil bleaching at various temperatures, and the values of X_m *and* K_L were obtained from the graph, where X_m is the slope and K_L the y-axis intercept. The values of X_m *and* K_L for GKS 2 at 60, 75 and 90°C are summarized in Table 4.8, which also shows the related correlation coefficients (R^2 values).

Table 4.8 Langmuir isotherm constants for the bleaching of rice bran oil using GKS 2 at various temperatures

Temperature (°C)	Langmuir constants		
	X_m (mg	K_L (kg/mg)	R^2
60	1.9701	0.1097	0.9528
75	2.0100	0.1326	0.9161
90	2.0627	0.1523	0.9066

The value of the correlation coefficients, R^2 from Tables 4.6 and 4.7 indicate that both Frundlich and Langmuir adsorption isotherm equation can be used to describe the adsorption process in these samples.

4.3.5 Desorption study

The desorption of adsorbed pigments from modified kaolin GKS 2 that had been used for bleaching rice bran oil was also investigated. After washing with hexane in order to dissolve any rice bran oil remaining in clay sample, the clay was eluted with ethanol, or 0.1M NaOH. The desorption values for pigment on modified kaolin GKS 2 using ethanol and 0.1 M NaOH were ~53% and ~90%, respectively. The high desorption percentage using 0.1 M NaOH shows that a high fraction of the pigment molecules were bound to acidic sites on the clay surface, which suggests an electrostatic interaction.

The FTIR result also indicated the possibly of an interaction between pigment and clay surface, since the spectrum of GKS 2 after bleaching showed new absorbance at ~1721 cm^{-1}, shifted from 1745 cm^{-1} the frequency of the ester carbonyl functional group on the chlorophyll molecule. Presumably the acidic sites on the clay interact with these electron-rich groups in the pigment molecule.

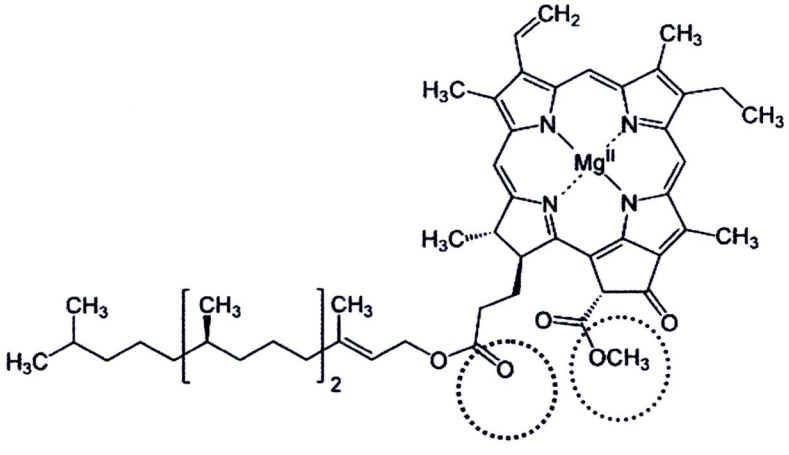

Electron- rich groups (polar groups) involved in the interaction with acidic site of surface clay

4.4 Physical properties of modified kaolin

The physical properties of natural kaolin (NK) and modified kaolin sample GKS 2 are summarized in Table 4.9

Table 4.9 Physical properties of NK and GKS 2

Parameters	NK	GKS 2
Apparent bulk density (g/cm^3)	1.12	0.3
Free moisture (2h, 105°C) (%)	15.2	5.0
Loss on ignition (pre-dried, 2h, 1000°C) (%)	13.5	12.9
pH (10% suspension)	6.5	3.0
Acidity	0.0	0.29
Specific surface area (BET) (m^2/g)	13.14	243.55

The apparent bulk density of the clay is inversely related its porosity: the more pore space in the clay, the lower its bulk density. After activation, the bulk density of the modified kaolin was ~3 fold lower than for the natural kaolin. Activation by grinding affects the clay structure, partly forming an amorphous phase. After chemical treatment this amorphous phase was leached and some components of the clay were dissolved. The particle size decreased and the specific surface area value increased ~18 fold.

Chemical treatment (acid activation) affects the acidity of clay. After acid treatment Lewis acidic sites in the clay decreased, cations were attacked and dissolved. However, an increase in the number of Brønsted acid sites increased the acidity of the clay, and the pH of a 10% suspension was 3.0.

4.5 Properties of bleached oil

Some properties of rice bran oil bleached using modified kaolin GKS 2 are summarized in Table 4.10. The bleached oil had a peroxide value 5.3 meq/kg, about 70% lower than in the degummed and neutralized crude rice bran oil because of the removal of oxidation products by the bleaching process. The acid value, however, was unchanged

by bleaching. This may be an affect of the low pH value of the modified kaolin suspension (~3.0). However, the acid value can be decreased in the deodorisation step. The color value in Lovibond units decreased, and the color of the bleached oil was pale yellow.

Table 4.10 Some properties of degumed and neutralized rice bran oil and bleached rice bran oil

Parameter	rice bran oil	bleached rice bran oil
Color(5¼")	70 Y/4.1R	35 Y/3.2 R
Chlorophyll contents (ppm)	12.0	0.062
Peroxide value (meq/kg)	18.8	5.3
Free fatty acid (% as oleic acid)	0.15	0.14

4.6 Oil retention by the adsorbent(OR)

In this work, the oil retention was calculated as follows:

Calculation :

% oil retention = [wt. extracted product ×100]/ wt. filtered cake

Percentage of oil retention of modified kaolin; GKS 2 is 39.27%

4.7 Oxidation during the bleaching of rice bran oil

The EPR spectra of rice bran oil before and after bleaching with activated kaolin are shown in Figure 4.23 along with a simulation of the spectrum from the bleached oil. Similar results were obtained with kaolins activated using sulphuric or oxalic acids. The spectrum observed with the oil before bleaching (Figure 4.23 (a)) consists of a single peak with g = 2.004 and 1st derivative peak-to-peak width of ~0.55 mT, It is, therefore, similar to that observed with many coloured materials of biological origin (e.g. humic substances (Cheshire, et al., 1985), seed testa (Hepburn, et al., 1986), roasted coffee (Pascual, et al., 2002)). After bleaching, the oil produced a spectrum containing hyperfine structure (Figure 4.23(b)), which could be simulated by a septet

pattern characteristic of six equivalent ^{1}H coupling constants of 0.545 mT. This is similar to the pattern produced in biological systems by the oxidation of α-tocopherol (e.g. Kalyanaraman, et al., 1995; Laranjinha and Cadenas, 1999)).

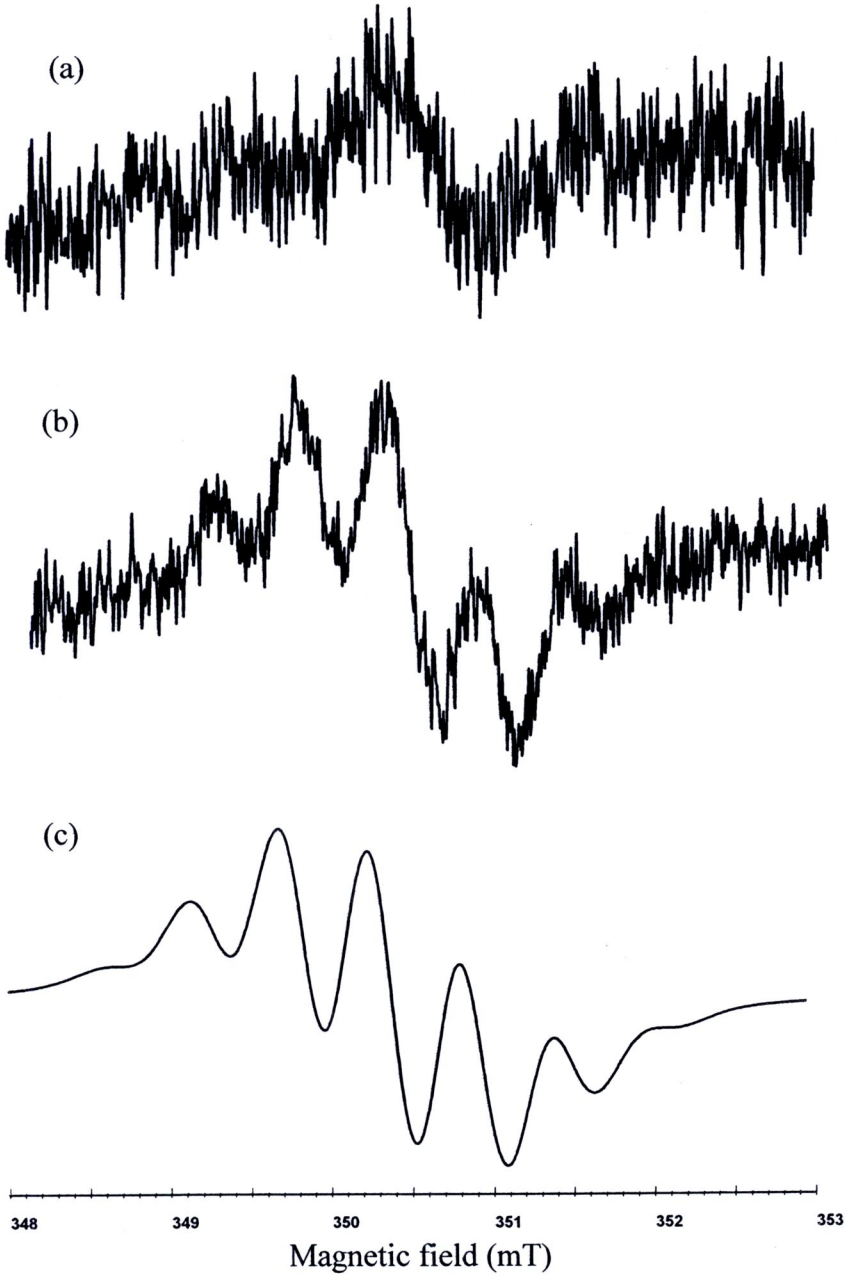

Figure 4.23 EPR spectrum of (a) degummed and neutralized rice bran oil, (b) rice bran oil after bleaching with modified kaolin, both recorded using 0.2 mT modulation amplitude, and (c) simulation assuming six equivalent ^{1}H hyperfine coupling constant of 0.545 mT.

Under higher resolution, additional structure was observed in the spectrum of the bleached oil (Figure 4.24 (a)), and this spectrum could be observed for more than one month after the bleaching treatment. Attempts to produce an accurate simulation of this spectrum with a single radical species were unsuccessful, and the nearest reproduction of the experimental spectrum is shown in Figure 4.24 (b).

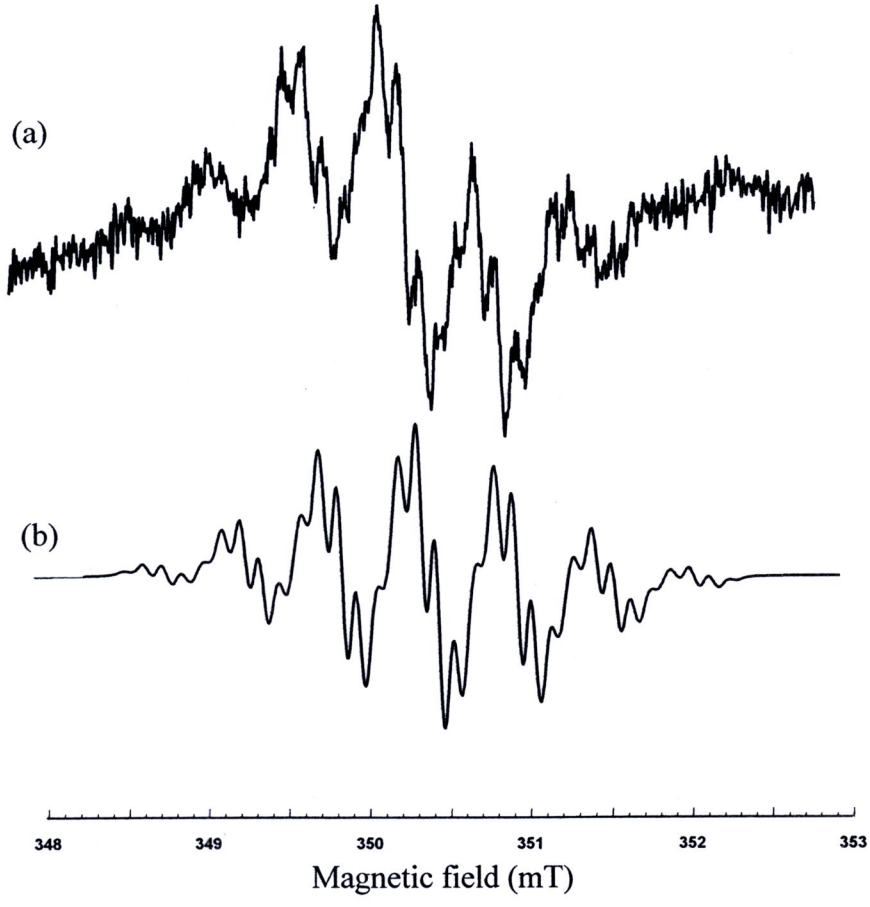

Figure 4.24 (a) 1st derivative EPR spectrum of bleached rice bran oil recorded using 0.1 mT modulation amplitude, (b) simulation based on 3 equivalent ^{1}H with 0.59 mT, 3 equivalent ^{1}H with 0.50 mT, 3 equivalent ^{1}H with 0.11 mT, and 1 ^{1}H with 0.13 mT

It would appear, therefore, that the EPR spectrum of bleached rice bran oil consists of more than one component, a major one of which is oxidised α-tocopherol. This is perhaps unsurprising, because vitamin E consists of four closely related tocopherols (α-,

β-, χ-, and δ-) and a similar number of tocotrienols, all of which on oxidation produce free radicals with distinct EPR spectra (Lehtovuori and Joela, 2002). What is surprising, however, is the stability of the radical species, since the tocopheroxyl radicals normally have limited stability. This results shows clearly that oxidation of such unstable species is very slow in the bleached oil, and is consistent with the long shelf-life of the bleached product.

4.8 Discussion

The XRD investigation of the natural Ranong kaolin sample shows that it is composed primarily of halloysite, but with significant amounts of kaolinite along with illite and quartz; goethite and microcline may also be present as minor impurities. However, discrimination between halloysite, kaolinite and illite was difficult, and could only be achieved by the use of oriented samples and a combination of chemical and heat treatments. This result here is qualitatively similar to that of Nuntiya and Prasanphan (2006), although these latter authors observed the additional presence of muscovite and appreciably greater amounts of quartz in the sample they investigated. However, local variations in the composition of kaolin deposits are not uncommon as a result of variations in the pre-weathering alteration history of parent rock, the degree of weathering, and variations in micro-environmental condition during kaolin formation (Duzgoren-Aydin, et al., 2002). Systematic changes in composition with particle size have been reported by Lombardi, et al. (1987) for kaolin deposits in Europe and North America, for example. Thus it is not surprising that there should be some differences between the samples of the kaolin used in the present work and that investigated by Nuntiya and Prasanphan (2006), even though they were obtained from the same general geographical region and are described by the same name.

The XRF results for the kaolin samples show that Si and Al are the dominant elements in the original kaolin, along with minor amounts of K and Fe, and only traces of other elements such as Mn. Acid treatments decreased the Al:Si and Fe:Si ratios and these decreases were much larger with ground samples. By combining these chemical data with the idealized chemical compositions of the phases identified by XRD, the fraction of the sample as kaolinite/halloysite decreases from ~85% in the original kaolin to ~40% in sample GKS. In the latter sample the main phase is probably amorphous silica

(≤50%) as suggested by an increase in the background in the 20-30°2θ range of the XRD patterns (**Section 4.1.1**), and the strong development of Si-O bands in the FTIR spectra (**Section 4.1.3**).

There are also some differences in the chemical composition of the present sample and that investigated by Nuntiya and Prasanphan (2006). Although differences in the SiO_2 and Al_2O_3 concentrations are minor, and the MnO concentrations are virtually identical, the Fe_2O_3 content of the present sample is much smaller. Therefore, this result suggests that there may be considerable variations in the concentrations of associated iron oxide phases in different samples from the Ranong deposit. The sandstone parent materials of kaolins derived from shale contain Fe in low to moderate amounts, there are moderate amounts of Fe in kaolins derived from granitic parent materials, and the highest amounts of Fe are found in kaolins derived from basalt (Hart, et al. 2003).

Because of the generally poorly crystalline nature of iron oxide phases associated with kaolin minerals, there may be correspondingly large variations in the sorption properties of different samples, especially if they are not subjected to chemical deferration procedures. The appreciable differences between the results from the present investigations and those of Frost, et al. (2001) are also an indication of different chemical behavior of samples from different origins. Thus careful attention must be paid to physical characterization when developing samples for practical uses, such as adsorbents in the food industry, and caution should be exercised in extrapolating properties from one specimen to another without detailed physical characterisation.

The tubular morphology observed in the SEM result from the unaltered sample (Figure 4.10) provides additional support for the XRD identification of halloysite, as an important component of this mineral. It is also consistent with the identification of halloysite by Nuntiya and Prasanphan (2006) in TEM investigations of their Ranong kaolin sample.

The specific surface area (S_{BET}) of of 13.1 m^2/g for the Ranong kaolin (Table 4.4) is appreciably smaller than the values reported for many other kaolin samples. For example, Hart, et al., (2000) found a mean value of 45.5 m^2/g (range 33.6 - 67.8 m^2/g)

for the S_{BET} for soil kaolins from ten sites in Thailand. The present value is, however, at the lower end of the range of S_{BET} values (11.4 - 46.8 m^2/g) reported by Cases, et al. (1986) for a range of kaolin samples. This result is consistent with the spectroscopic evidence that the Ranong kaolin is a reasonably well-ordered sample and the analysis of the XRD data using the Scherrer formula. The wide range of S_{BET} values for natural kaolin samples also suggests that appreciably different sorption properties might be expected for different specimens of this mineral. The low S_{BET} value for Ranong kaolin is also probably a major reason for the poor performance of acid activated samples of the unground mineral in the bleaching of rice bran oil (Table 4.5). However, by first disrupting the kaolin mineral structure by grinding, it was possible to produce acid activated structures with high surface area and appropriate pore size distributions for effective oil decolorisation.

The XRD diffractogram of unground kaolin after sulfuric acid treatment showed only slight changes from that of the untreated kaolin, even under strongly acidic conditions (Figure 4.3(a-c)), indicating the stability of the kaolinite and halloysite components to mineral acid, presumably because of the strong hydrogen bonds in the structure. Grinding, however, (partially) destroyed the kaolin mineral structures and decreased structural order. This was seen by a decrease in intensity of the XRD peaks associated with kaolinite/halloysite(Figure 4.3), a weakening of the O-H stretching bands in the FTIR spectra (Figure 4.4) and a change in the shape of the EPR spectral components assigned to Fe^{3+} (Figure 4.6). Furthermore, a decrease in particle size could be seen in SEM images (Figure 4.11(a)), and the specific surface area and total pore volume increased appreciably (Table 4.4). Along with an increase in the background in the 20-30°2θ range of the XRD trace (Figure 4.3(d)), these observations are all consistent with the formation of poorly crystalline or amorphous phases. They are also consistent with the NMR study of Temuujin, et al. (2001), who reported destruction of the octahedral layers of kaolinite by prolonged grinding.

Chemical treatments of the ground kaolin sample resulted in large increases in the specific surface area and the total pore volume (Table 4.4), and this was accompanied by a major decrease in the Al contents (Table 4.2). Apart from the peak at ~26.74° 2θ, which probably corresponds to quartz, there was an appreciable reduction in intensity in

all regions of the XRD spectrum, consistent with breakdown or loss of crystallinity in all of the aluminosilicate mineral phases. Aluminium was extracted from the phases produced by grinding-induced breakdown of the kaolin mineral structures, and a Si-rich phase remained. This is probably amorphous silica, an interpretation which is supported by the strong development of Si-O bands in the FTIR spectra. However, although the peaks corresponding to the kaolinite/halloysite minerals were very weak in the XRD spectra, they were still quite sharp (Table 4.1), suggesting that the residual fraction of these minerals is relatively unaltered.

The FTIR spectroscopic results indicate that –OH groups were lost as a result of grinding, presumably as a result of dehydroxylation caused by heat generated during the grinding process. Since these groups are associated with the surface of the octahedral sheet, there would inevitably be a major change in the coordination environment of the Al and a decrease in the number of hydrogen bonds that hold together the individual aluminosilicate sheets. This dehydroxylation was accompanied by a breakdown of the structure, from which alumina could be removed by subsequent acid treatments. These results also indicate that probably ~50% of the remaining material was in the form of amorphous silica.

In contrast to the other techniques, which provided evidence for changes to the main mineral components, EPR spectroscopy gave an insight into the structural changes that affected the Fe, Mn and free radical components, all of which make relatively minor contributions to the overall composition of the kaolin. However, because paramagnetic centres are often associated with specific reactivity, as a result of their ability to undergo redox reactions, EPR spectroscopy may provide insight into the chemical nature of structural sites involved in specific reactions by acting as a sensitive probe into the chemical environments of these various paramagnetic entities. In the EPR spectra of the kaolin, the low field features from Fe^{3+} in octahedral sites within the aluminosilicate structure were sensitive to grinding, but not to acid treatments. In contrast the signal from Mn was unaffected by grinding, but sensitive to acid treatments of both the ground and unground samples.

The observation that grinding increased the fraction of the Fe^{3+} that is associated with sites lacking long range structural order provides support for the conclusion based on

the XRD results that this treatment caused a major reduction in the content of crystalline aluminosilicate phases. The location of the Fe^{3+} ions in octahedral sites is also supported by the FTIR results which show a major loss of –OH groups, which form the surface of the octahedral sheet. The lack of any corresponding sensitivity of the Mn signal to grinding is strong evidence for the Mn being located in different types of site to the Fe, especially since it was sensitive to acid treatment of the mineral samples. In addition, the broad absorptions from magnetically-interacting ions, along with those from the free radical components, seemed not to be affected significantly by grinding. The absence of a major increase in the free radical signal as a result of the grinding is somewhat surprising, since such treatment is well-known to generate free radical defects in mineral structures (e.g. (Hart, et al. 2003)).

The absence of any observed effect of acid treatment on the Fe^{3+} signal in the unground kaolin indicates that removal of (surface-bound) material by acid treatment had no effect on the distribution of structural Fe, nor on the long range order of the kaolinite/halloysite mineral phase. Again this result is in agreement with that obtained by XRD of the same samples. In contrast to the result with unground kaolin, acid treatment of the ground kaolin increased the $Fe_{(II)}$ contribution to the total Fe^{3+} signal, although it still remained much lower than in the unground specimens. However, the most likely explanation for this latter observation is that some of the most poorly ordered Fe-containing phases generated by grinding were removed by acid treatment, and not that acid stimulated some recrystallization of the mineral.

The signal centred on the free spin value (~350 mT) overlays a broad background, which corresponds to magnetically interacting paramagnetic ions. Such a signal is often assigned to poorly-crystalline iron oxides (e.g. Goodman and Hall, 1994), which are a common feature of natural kaolin samples (Fysh, et al. 1983), but it could correspond to any phase containing domains in which coupling occurs between unpaired electrons on neighbouring paramagnetic centres. Examination of the EPR spectra derived from the unground kaolin samples (Figure 4.6) shows that there was a reduction in the relative intensity of the broad component as a result of sulfuric acid treatment, which probably corresponds to the removal of associated poorly crystalline oxide phases. However, this component retained appreciable intensity after acid treatment, indicating the presence of magnetically-interacting ions in the aluminosilicate structure, either in kaolinite/

halloysite, or a more-Fe-rich mineral phase. This conclusion is supported by the XRF results, which indicate only partial removal of Fe by acid treatments.

All of the EPR spectra contain features attributable to interactions of unpaired electrons with ^{55}Mn nuclei, identifiable by the characteristic sextet structure from its I=5/2 nucleus. Although not a common substituent of kaolinites, there have been previous reports of EPR spectra of Mn in natural kaolin specimens, though often assigned to the presence of impurity phases containing Mn^{2+} (*e.g.* Sengupta et al., 2006), or Mn^{2+} adsorbed on kaolinite surfaces (*e.g.* McBride et al., 1975). The ^{55}Mn hyperfine splitting of ~9.3 mT is typical of that for Mn^{2+} octahedrally coordinated to oxygen atoms, as for example in $Mn(H_2O)_6^{2+}$ on the exchange sites in clay minerals (McBride et al., 1975) or in oxide crystals, such as CaO or CdO (Title, 1963). However, the lack of any loss of intensity as a result of acid treatments, combined with its similar concentrations in the XRF measurements before and after acid treatment, would appear to exclude the adsorption of Mn^{2+} ions on surface sites as the source of the Mn signal in the original kaolin sample. Also, the different behaviour of Fe and Mn in response to physical and chemical treatments indicates that these ions occur in different types of mineral site. Thus since the Fe is clearly associated with the octahedral sheet of the kaolin minerals, it would appear that the Mn must be located elsewhere, either in the tetrahedral sheet or associated with a different mineral phase. Although it is not possible to specifically exclude the latter interpretation, XRD provided no evidence to support the presence of significant quantities of any specific associated mineral phase in which Mn could be present in a magnetically dilute form, which is necessary for the observation of the ^{55}Mn hyperfine structure.

Further support for the conclusion that the Mn is located in positions in the lattice that are different from those that are occupied by the Fe^{3+} ions is provided by the observation of changes in the Mn signal on re-suspension in solutions of different pH values of samples that had previously been modified by combined physical and chemical treatments. Therefore, it would appear by a process of elimination that the Mn is located in the tetrahedral sheet, a conclusion which is in direct contrast to the location of V^{4+}, for which Gehring, et al. (1993) found strong evidence for it being located primarily in the octahedral sheet. If it is indeed in the tetrahedral sheet, it is also probable that the Mn in this kaolin is in the Mn^{4+} oxidation state. The main free radical

signal corresponds to the A-centre reported previously for defects induced by exposure to γ-irradiation. Its relative insensitivity to prolonged grinding is consistent with the assignment to an electron hole on an O atom associated with Si, and adds support to the proposed use of this resonance for measuring the radiation history of the sample (Clozel, et al., 1990). The ^{27}Al hyperfine structure that is associated with the B-centre was not resolved in the ground samples, consistent with grinding-induced damage having the major effect on the surface of the octahedral sheet.

A 2nd derivative recording of the most intense free radical peak (i.e. the $g_{\perp}$ feature of the defect centre) showed that it contains more than one component (Figure 4.8). Clozel, et al. (1994) observed the presence of three distinct radiation-induced radical centres in kaolinites in spectra recorded at Q-band frequencies (~35 GHz), but it is unusual for such resolution to be observed at lower frequencies. Figure 4.8 also shows that there was some change in the relative intensities of the peaks resolved in the 2nd derivative spectra. However, part of this signal could be located in associated minerals, such as quartz, where radiation-induced defects are well-known (e.g. Weeks, 1956).

Although acid activation of the original kaolin sample produced disappointing results for the decolorisation of rice bran oil, much better performance was obtained when the sample was ground before acid activation (Table 4.5). A combination of grinding and treatment with 2 M H_2SO_4 acid produced a modified kaolin with decolorisation capacity comparable to that of a commercial (bentonite) bleaching clay (79.6% versus 81.9%). Although this combined physical and chemical treatment gave the best performance in the current experiments, this is not necessarily the optimum performance for a modified kaolin. Improvements might be possible by refinements to the grinding and/or acid treatment procedures. Indeed a modification of the surface of the modified kaolin by resuspension in pH 2 sulfuric acid resulted in an increase in the decolorisation capacity to 80.9% (Table 4.6).

The extent of pigment adsorption from the rice bran oil is related to the surface properties of the modified kaolin samples, and these were in turn strongly influenced by both the concentration and chemical nature of the acid used for the acid treatment. With both sulfuric and oxalic acids, there was a fairly narrow range of concentrations that produced optimum decolorisation capacity. These were around 2 M - 2.3 M for sulfuric

acid and 0.7 M for oxalic acid (Table 4.5). The different optimum concentrations for the two acids is probably a reflection of their different modes of action, with the chelation ability of oxalic acid making it a more efficient molecule for metal ion removal. Indeed the EPR spectra show that the Mn component is influenced to a much greater extent by oxalic acid than it is by sulfuric acid. Thus if as proposed above the Mn is associated with the tetrahedral sheet, then it is the surface of this sheet (i.e. the silica surface) that is most affected by the acid treatments of the ground kaolin samples.

After being used for rice bran oil bleaching, the kaolin developed a green colour from adsorbed pigment molecules. These adsorbed pigments were not extracted by hexane, and only partially extracted by ethanol, this result indicating a strong interaction between the mineral and pigment components. However, treatment with 0.1 M NaOH removed 90% of the pigment molecules. Thus refinement of the extraction treatment to allow regeneration of the modified kaolin for reuse is a distinct possibility, and one which adds greatly to the economics of replacing bentonite bleaching clays by modified kaolins for vegetable oil decolorisation.

Finally, investigations of the bleached rice bran oils indicate that some oxidation accompanies the bleaching process, an observation that is unsurprising since high temperatures are involved. However, the peroxide value was ~70% lower than in the unbleached oil. In the bleached oil, the EPR spectra are consistent with the presence of tocopheroxyl radicals, which are presumably produced by the oxidation of vitamin E, a major group of antioxidant molecules in vegetable oils. These radicals were able to be observed some four weeks after the oil bleaching, thus demonstrating that the bleached oil is able to stabilize them against further oxidation. The high stability of rice bran oil produced by decolorisation using modified kaolin is encouraging for the possible generation of products with extended shelf-lives.